

---

# Automatic Symmetry Discovery with Lie Algebra Convolutional Network

---

**Nima Dehmamy**  
Northwestern University  
nimadt@bu.edu

**Robin Walters**  
Northeastern University

**Yanchen Liu**  
Northeastern University

**Dashun Wang**  
Northwestern University

**Rose Yu**  
University of California San Diego

## Abstract

Existing equivariant neural networks for continuous groups require discretization or group representations. All these approaches require detailed knowledge of the group parametrization and cannot learn entirely new symmetries. We propose to work with the Lie algebra (infinitesimal generators) instead of the Lie group. Our model, the Lie algebra convolutional network (L-conv) can learn potential symmetries and does not require discretization of the group. We show that L-conv can serve as a building block to construct any group equivariant architecture. We discuss how CNNs and Graph Convolutional Networks are related to and can be expressed as L-conv with appropriate groups. We also derive the MSE loss for a single L-conv layer and find a deep relation with Lagrangians used in physics, with some of the physics aiding in defining generalization and symmetries in the loss landscape. Conversely, L-conv could be used to propose more general equivariant ansätze for scientific machine learning.

## 1 Introduction

Encoding symmetries into a machine learning (ML) architecture (Cohen & Welling, 2016a; Bogatskiy et al., 2020; Maron et al., 2020; Bronstein et al., 2021) can reduce data requirements and improve generalization, while significantly reducing the number of model parameters (Cohen et al., 2019b; Cohen & Welling, 2016b; Ravanbakhsh et al., 2017; Ravanbakhsh, 2020). For instance, Convolutional Neural Networks (CNN) (LeCun et al., 1989, 1998) incorporate translation symmetry into the architecture. General principles for constructing group equivariant networks were introduced in Cohen & Welling (2016b), Kondor & Trivedi (2018), and Cohen et al. (2019b). Many existing works on equivariant architectures focus on *finite groups* such as permutations Hartford et al. (2018); Ravanbakhsh et al. (2017); Zaheer et al. (2017), 90 degree rotations Cohen et al. (2018) or dihedral groups  $D_N$   $E(2)$  Weiler & Cesa (2019).

For a continuous group, the number of group elements is infinite. To incorporate them into the architecture, existing approaches either discretize the group Weiler et al. (2018a,b); Cohen & Welling (2016a), or use a truncated sum over irreps Weiler & Cesa (2019); Weiler et al. (2018a) via spherical harmonics in Worrall et al. (2017) or more general Clebsch-Gordon coefficients Kondor et al. (2018); Bogatskiy et al. (2020). These approaches are prone to approximation error. Both parametrizing Lie groups for sampling and finding irreps are computationally expensive.

Another approach taken in Finzi et al. (2020) approximates the integral over the Lie group by Monte Carlo sampling. However, their approach is quite involved, using the matrix logarithm and exponential to define a distance function used to obtain a sampling neighborhood for each point. Finzi et al. (2021) provides a unified approach for encoding continuous groups multi-layer perceptrons (MLP).

Their method requires knowledge of the group, encoding its irreducible representations, and solving a set of symmetry constraints.

**Contributions** Existing approaches require hand-coding group representations or elements into the architecture. Each Lie group has a different parametrization and this task is quite tedious. Our goal is to significantly simplify this process. Our intuition stems from the fact that Lie groups can be constructed from a set of infinitesimal generators, called the Lie algebra. The Lie algebra has a finite basis, assuming the group is not infinite-dimensional (e.g. in quantum or conformal field theory (Belavin et al., 1984)). By working with the Lie algebra basis, we avoid having to encode an infinite group by discretizing or summing over irreps. The other benefit of this approach is that all Lie algebras have the same general structure and hence can be implemented the same way. Additionally, for most symmetries we can expect the number of Lie algebra basis elements to be small and we could make them learnable parameters. Hence, our architecture is potentially capable of learning symmetries in data without imposing inductive biases.

We propose Lie Algebra Convolutional Network (**L-conv**), a novel architecture that can automatically discover symmetry from data. Our main contributions can be summarized as follows:

- We propose the Lie algebra convolutional network (**L-conv**), a building block for constructing group equivariant architectures.
- We show that multi-layer L-conv can approximate group convolutional layers, including CNN, and find graph convolutional networks to be a special case of L-conv.
- The Lie algebra generators in our L-conv can be learned to automatically discover symmetries.
- We find that MSE loss function for L-conv generalizes important Lagrangians in physics.
- We find generalization error and equivariance in the loss landscape can be expressed as Euler-Lagrange equations and Noether currents, transferring ideas from physics to ML.

## 2 Background

We now review core concepts which we build upon: equivariance, group convolution and Lie algebras.

**Notations** Unless explicitly stated,  $a$  in  $A^a$  is an index, not an exponent. We use the Einstein notation, where a repeated upper and lower index are summed over, meaning  $A^a B_{ab} = \sum_a A^a B_{ab} = [AB]_b$ .

**Equivariance** Let  $\mathcal{S}$  be a topological space on which a Lie group  $G$  (continuous group) acts from the left, meaning for all  $\mathbf{x} \in \mathcal{S}$  and  $g \in G$ ,  $g\mathbf{x} \in \mathcal{S}$ . We refer to  $\mathcal{S}$  as the base space. Let  $\mathcal{F}$ , the “feature space”, be the vector space  $\mathcal{F} = \mathbb{R}^m$ . Each data point is a feature map  $f : \mathcal{S} \rightarrow \mathcal{F}$ . For instance, in images  $f(\mathbf{x}) \in \mathcal{F}$  are the colors at pixel  $\mathbf{x} \in \mathcal{S}$ . The action of  $G$  on the input of  $f$  induces an action on feature maps. For  $u \in G$ , the transformed features  $u \cdot f$  are given by

$$u \cdot f(\mathbf{x}) = f(u^{-1}\mathbf{x}). \quad (1)$$

Denote the space of all functions from  $\mathcal{S}$  to  $\mathcal{F}$  by  $\mathcal{F}^{\mathcal{S}}$ , so that  $f \in \mathcal{F}^{\mathcal{S}}$ . Let  $F$  be a mapping to a new feature space  $\mathcal{F}' = \mathbb{R}^{m'}$ , meaning  $F : \mathcal{F}^{\mathcal{S}} \rightarrow \mathcal{F}'^{\mathcal{S}}$ . We say  $F$  is *equivariant* under  $G$  if  $G$  acts on  $\mathcal{F}'$  and for  $u \in G$

$$u \cdot (F(f)) = F(u \cdot f). \quad (2)$$

**Group Convolution** Kondor & Trivedi (2018) showed that  $F$  is a linear equivariant map if and only if it performs a group convolution (G-conv). To define G-conv, we first lift  $\mathbf{x}$  to elements in  $G$  (Kondor & Trivedi, 2018). To do the lift, we pick an origin  $\mathbf{x}_0 \in \mathcal{S}$  and replace each point  $\mathbf{x} = g\mathbf{x}_0$  by  $g$ . We will often drop  $\mathbf{x}_0$  for brevity and write  $f(g) \equiv f(g\mathbf{x}_0)$ . Let  $\kappa : G \rightarrow \mathbb{R}^{m'} \otimes \mathbb{R}^m$  be a linear transformation from  $\mathcal{F}$  to  $\mathcal{F}'$ . G-conv is defined as

$$[\kappa \star f](g) = \int_G \kappa(g^{-1}v)f(v)dv = \int_G \kappa(v)f(gv)dv, \quad (3)$$

where for brevity, we are denoting the Haar measure on  $G$  as  $dv \equiv d\mu(v)$ .

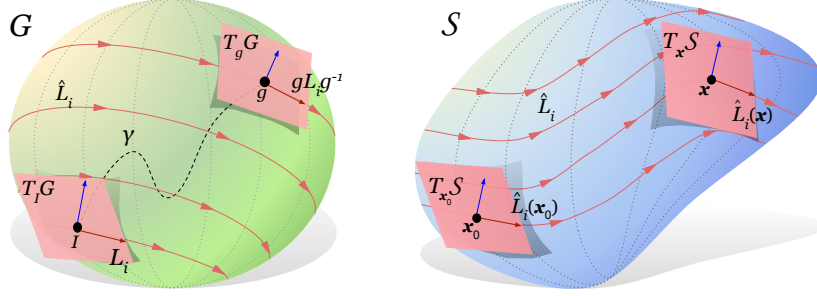


Figure 1: **Lie group and Lie algebra:** Illustration of the group manifold of a Lie group  $G$  (left). The Lie algebra  $\mathfrak{g} = T_I G$  is the tangent space at the identity  $I$ .  $L_i$  are a basis for  $T_I G$ . If  $G$  is connected,  $\forall g \in G$  there exist paths like  $\gamma$  from  $I$  to  $g$  and  $g$  can be written as a path-ordered integral  $g = P \exp[\int_\gamma dt^i L_i]$ . **Base space** Right is a schematic of the base space  $\mathcal{S}$  as a manifold. The lift  $x = gx_0$  takes  $x \in \mathcal{S}$  to  $g \in G$ , and maps the tangent spaces  $T_x \mathcal{S} \rightarrow T_g G$ . Each Lie algebra basis  $L_i \in \mathfrak{g} = T_I G$  generates a vector field  $\hat{L}_i$  on the tangent bundle  $TG$  via the pushforward  $\hat{L}_i(g) = gL_i g^{-1}$ . Via the lift,  $L_i$  also generates a vector field  $\hat{L}_i = \hat{L}_i^\alpha(x) \partial_\alpha = [gL_i x_0]^\alpha \partial_\alpha$ .

**Equivariance of G-conv** As shown in Kondor & Trivedi (2018), G-conv is equivariant. The equivariance of equation 3 can be readily checked using equation 1. For  $w \in G$  we have

$$\begin{aligned} [\kappa \star w \cdot f](g) &= \int_G \kappa(v) w \cdot f(gv) dv = \int_G \kappa(v) f(w^{-1} gv) dv \\ &= [\kappa \star f](w^{-1} g) = w \cdot [\kappa \star f](g) \end{aligned} \quad (4)$$

Most existing literature on equivariance implements  $\int_G$  by discretizing the group or summing over irreducible representations. We take a different approach and instead use the infinitesimal generators of the group. While a Lie group  $G$  is infinite, usually it can be generated using a small number of infinitesimal generator, comprising its ‘‘Lie algebra’’. We use the Lie algebra to introduce a building block from which any G-conv can be constructed. Next, we review core concepts about Lie algebras. Figure 1 shows an illustration of a Lie group, Lie algebra and the concept we discuss below.

**Lie algebra** Let  $G$  be a Lie group, which includes common continuous groups. Group elements  $u \in G$  infinitesimally close to the identity element  $I$  can be written as  $u \approx I + \epsilon^i L_i$  (note Einstein summation), where  $L_i \in \mathfrak{g}$  with the Lie algebra  $\mathfrak{g} = T_I G$  is the tangent space of  $G$  at the identity element. The Lie algebra has the property that it is closed under a Lie bracket  $[\cdot, \cdot] : \mathfrak{g} \times \mathfrak{g} \rightarrow \mathfrak{g}$

$$[L_i, L_j] = c_{ij}^k L_k, \quad (5)$$

which is skew-symmetric and satisfies the Jacobi identity. Here the coefficients  $c_{ij}^k \in \mathbb{R}$  or  $\mathbb{C}$  are called the structure constants of the Lie algebra. For matrix representations of  $\mathfrak{g}$ ,  $[L_i, L_j] = L_i L_j - L_j L_i$  is the commutator. The  $L_i$  are called the infinitesimal generators of the Lie group.

**Exponential map** If the manifold of  $G$  is connected<sup>1</sup>, an exponential map  $\exp : \mathfrak{g} \rightarrow G$  can be defined such that  $g = \exp[t^i L_i] \in G$ . For matrix groups, if  $G$  is connected and compact, the matrix exponential is such a map and it is surjective. For most other groups (except  $GL_d(\mathbb{C})$  and nilpotent groups) it is not surjective. Nevertheless, for any connected group every  $g \in G$  can be written as a product  $g = \prod_a \exp[t_a^i L_i]$  (Hall, 2015). Making  $t_a^i$  infinitesimal steps  $dt^i(s)$  tangent to a path  $\gamma$  from  $I$  to  $g$  on  $G$  yields the surjective path-ordered exponential in physics, denoted as  $g = P \exp[\int_\gamma dt^i L_i]$  (SI A, and see Time-ordering in Weinberg (1995, p143)).

**Pushforward**  $L_i \in T_I G$  can be pushed forward to  $\hat{L}_i(g) = gL_i g^{-1} \in T_g G$  to form a basis for  $T_g G$ , satisfying the same Lie algebra  $[\hat{L}_i(g), \hat{L}_j(g)] = c_{ij}^k \hat{L}_k(g)$ . The manifold of  $G$  together with the set of all  $T_g G$  attached to each  $g$  forms the tangent bundle  $TG$ , a type of fiber bundle (Lee et al., 2009).  $\hat{L}_i$  is a vector field on  $TG$ . The lift maps  $\hat{L}_i$  to an equivalent vector field on  $T\mathcal{S}$ , which we will also denote by  $\hat{L}_i$ . Figure 1 illustrates the flow of these vector fields on  $TG$  and  $T\mathcal{S}$ .

<sup>1</sup>When  $G$  has multiple connected components, these results hold for the component containing  $I$ , and generalize easily for multi-component groups such as  $\mathbb{Z}_k \otimes G$  (Finzi et al., 2021).

### 3 Lie Algebra Convolutional Network

The Lie algebra basis  $L_i \in \mathfrak{g}$  can be used to construct the Lie group  $G$  using the exponential map. Similarly, we show that G-conv layers can be constructed using a more basic architecture utilizing the Lie algebra. The key idea is to approximate the kernel  $\kappa(u)$  using localized kernels which can be constructed using the Lie algebra (Fig. 2). This process closely mimics the universal approximation theorem of neural networks. Concretely, we will use the Lie algebra to expand G-conv equation 3 near the identity  $I$ . This yields basic building blocks from which an arbitrary G-conv can be constructed.

Let  $\delta_\eta(u) \in \mathbb{R}$  denote a normalized *localized kernel*, meaning  $\int_G \delta_\eta(g) dg = 1$ , and with support on a small neighborhood of size  $\eta$  near  $I$  (i.e.,  $\delta_\eta(I + \epsilon^i L_i) \rightarrow 0$  if  $\|\epsilon\|^2 > \eta^2$ ). Let  $\kappa_0(u) = W^0 \delta_\eta(u)$ , where  $W^0 \in \mathbb{R}^{m'} \otimes \mathbb{R}^m$  are constants. The localized kernels  $\kappa_0$  can be used to approximate G-conv. We first derive the expression for a G-conv whose kernel is  $\kappa_0$ .

**Linear expansion of G-conv with localized kernel** We can expand a G-conv whose kernel is  $\kappa_0(u) = W^0 \delta_\eta(u)$  in the Lie algebra of  $G$  to linear order. With  $v_\epsilon = I + \epsilon^i L_i$ , we have (see SI A, equation 26)

$$\begin{aligned} Q[f](g) &= [\kappa_0 \star f](g) = \int_G dv \kappa_0(v) f(gv) = \int_{\|\epsilon\| < \eta} dv_\epsilon \kappa_0(v_\epsilon) f(gv_\epsilon) \\ &= W^0 \int d\epsilon \delta_\eta(v_\epsilon) \left[ f(g) + \epsilon^i g L_i \cdot \frac{d}{dg} f(g) + O(\epsilon^2) \right] \\ &= W^0 \left[ I + \bar{\epsilon}^i g L_i \cdot \frac{d}{dg} \right] f(g) + O(\eta^2) \end{aligned} \quad (6)$$

where  $W^0 \in \mathbb{R}^{m'} \otimes \mathbb{R}^m$ , and using  $\int_G \delta_\eta(g) dg = \int d\epsilon \delta_\eta(v_\epsilon) = 1$  and  $\epsilon^i \in \mathbb{R}^m \otimes \mathbb{R}^m$ , we have defined

$$\bar{\epsilon}^i = \int d\epsilon \delta_\eta(v_\epsilon) \epsilon^i \in \mathbb{R}^m \otimes \mathbb{R}^m. \quad (7)$$

Note that because  $\|\epsilon\| < \eta$  we also have  $\|\bar{\epsilon}\| < \eta$  (SI A, equation 27). Here  $d\epsilon$  is the integration measure on the Lie algebra  $\mathfrak{g} = T_I G$  induced by the Haar measure  $dv_\epsilon$  on  $G$ .

**Interpreting the derivatives** In a matrix representation of  $G$ , we have  $g L_i \cdot \frac{df}{dg} = [g L_i]_\alpha^\beta \frac{df}{dg^\beta} = \text{Tr} \left[ [g L_i]^T \frac{df}{dg} \right]$ . This can be written in terms of partial derivatives  $\partial_\alpha f(\mathbf{x}) = \partial f / \partial x^\alpha$  as follows. Using  $\mathbf{x}^\rho = g^\rho_\sigma \mathbf{x}_0^\sigma$ , we have  $\frac{df(g \mathbf{x}_0)}{dg^\beta} = \mathbf{x}_0^\beta \partial_\alpha f(\mathbf{x})$ , and so

$$\hat{L}_i f(\mathbf{x}) \equiv g L_i \cdot \frac{df}{dg} = [g L_i]_\beta^\alpha \mathbf{x}_0^\beta \partial_\alpha f(\mathbf{x}) = [g L_i \mathbf{x}_0] \cdot \nabla f(\mathbf{x}) \quad (8)$$

Hence, for each  $L_i$ , the pushforward  $g L_i g^{-1}$  generates a flow on  $\mathcal{S}$  through the vector field  $\hat{L}_i \equiv g L_i \cdot d/dg = [g L_i g^{-1} \mathbf{x}]^\alpha \partial_\alpha$  (Fig. 1).

**Lie algebra convolutional (L-conv) layer** Equation 6 states that for a kernel localized near identity the effect of the kernel can be summarized in  $W^0$  and  $\bar{\epsilon}^i \hat{L}_i$ . It is important to note that we do not need to perform the integral over  $G$  explicitly anymore. Instead of working with a kernel  $\kappa_0$ , we only need to specify  $W^0$  and  $\bar{\epsilon}^i$ . The construction in equation 6 turns out to be the basic building block of G-conv, as we show below. Hence, in general, we define the Lie algebra convolution (L-conv) as follows

$$\begin{aligned} Q[f](\mathbf{x}) &= W^0 \left[ I + \bar{\epsilon}^i \hat{L}_i \right] f(\mathbf{x}) \\ &= W^0 \left[ I + \bar{\epsilon}^i [g L_i \mathbf{x}_0]^\alpha \partial_\alpha \right] f(\mathbf{x}) \end{aligned} \quad (9)$$

Being an expansion of G-conv, L-conv inherits the equivariance of G-conv, as we show next.

**Proposition 1** (Equivariance of L-conv). *With assumptions above, L-conv is equivariant under  $G$ .*

*Proof:* First, note that the components of  $\hat{L}_i$  transform as  $[\hat{L}_i(v \mathbf{x})]^\alpha = [v g L_i \mathbf{x}_0]^\alpha = v^\alpha_\beta \hat{L}_i(\mathbf{x})^\beta$ , while the partial transforms as  $\partial / \partial [v \mathbf{x}]^\alpha = [v^{-1}]^\gamma_\alpha \partial_\gamma$ . As a result in  $\hat{L}_i = [g L_i \mathbf{x}_0]^\alpha \partial_\alpha$  all factors of

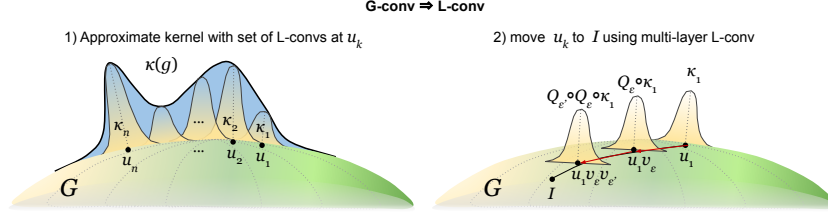


Figure 2: Sketch of the procedure for approximating G-conv using L-conv. First, the kernel is written as the sum of a number of localized kernels  $\kappa_k$  with support around  $u_k$  (left). Each of the  $\kappa_k$  is then moved toward identity by composing multiple L-conv layers  $Q_{\epsilon'} \circ Q_{\epsilon} \dots \kappa_k$  (right).

$v$  cancel. In fact,  $\hat{L}_i \in T\mathcal{S}$  is a vector field (i.e. 1-tensor) and all vectors fields are independent of the basis, meaning for  $v \in G$ ,  $\hat{L}_i(v\mathbf{x}) = \hat{L}_i(\mathbf{x})$ . Plugging into equation 9, for  $w \in G$

$$\begin{aligned}
w \cdot Q[f](\mathbf{x}) &= Q[f](w^{-1}\mathbf{x}) = W^0 \left[ I + \bar{\epsilon}^i \hat{L}_i(w^{-1}\mathbf{x}) \right] f(w^{-1}\mathbf{x}) \\
&= W^0 \left[ I + \bar{\epsilon}^i \hat{L}_i(g) \right] f(w^{-1}\mathbf{x}) = W^0 \left[ I + \bar{\epsilon}^i \hat{L}_i(g) \right] w \cdot f(\mathbf{x}) \\
&= Q[w \cdot f](\mathbf{x})
\end{aligned} \tag{10}$$

which proves L-conv is equivariant.  $\square$

Next, we provide some explicit example of the form of L-conv for familiar continuous symmetries.

### 3.1 Interpretation and Examples

Using equation 8 we can calculate the form of L-conv for specific groups (details in SI A.2). For **translations**  $G = T_n = (\mathbb{R}^n, +)$  we find the generators become simple partial derivatives  $\hat{L}_i = \partial_i$  (SI A.2.2), yielding  $f(\mathbf{x}) + \epsilon^\alpha \partial_\alpha f(\mathbf{x})$ . For **2D rotations** (SI A.2.1) we find  $\hat{L} \equiv (x\partial_y - y\partial_x) = \partial_\theta$ , which in physics is called the angular momentum operator about the z-axis in quantum mechanics and field theories. For rotations with scaling, **Rotation and scaling**  $G = SO(2) \times \mathbb{R}^+$ , we have two  $L_i$ , one  $\hat{L}_\theta = \partial_\theta$  from  $so(2)$  and a scaling with  $L_r = I$ , yielding  $\hat{L}_r = x\partial_x + y\partial_y = r\partial_r$ . Next, we discuss the form of L-conv on discrete data.

### 3.2 Approximating G-conv using L-conv

L-conv can be used as a basic building block which can be combined to make more G-conv with more general kernels. Figure 2 sketches the argument described here (see SI A.1 for more discussion).

**Theorem 1** (G-conv from L-convs). *G-conv equation 3 can be approximated using L-conv layers.*

*Proof:* The procedure involves two steps, as illustrated in Fig. 2: 1) approximate the kernel using localized kernels as the  $\delta_\eta$  in L-conv; 2) move the kernels towards identity using multiple L-conv layers. The following lemma outline the details.  $\square$

**Lemma 1** (Approximating the kernel). *Any kernel  $\kappa$  can be approximated using a set of kernels with  $\eta$  support to arbitrary accuracy.*

*Proof:* This simply follows from the universal approximation theorem for neural networks (Hornik et al., 1989; Cybenko, 1989) and the same approximation errors apply.  $\delta_\eta(g)$  can be written as the sum of two sigmoid functions  $\delta_\eta(g) = \text{sig}(v_\eta g) + \text{sig}(v_\eta^{-1}g)$ . Thus, we can approximate any kernel as  $\kappa(g) \approx \sum_k \kappa_k(g)$  where the local kernels  $\kappa_k(g) = c_k \delta_\eta(u_k^{-1}g)$  have support only on an  $\eta$  neighborhood of  $u_k \in G$ . Here  $c_k \in \mathbb{R}^{m'} \otimes \mathbb{R}^m$  are constants and  $\delta_\eta(u)$  is as in equation 6. Using this, G-conv equation 3 becomes

$$[\kappa \star f](g) = \sum_k c_k \int dv \delta_\eta(u_k^{-1}v) f(gv) = \sum_k c_k [\delta_\eta \star f](gu_k). \tag{11}$$

The kernels  $\kappa_k$  are localized around  $u_k$ , whereas in L-conv the kernel is around identity. We can compose L-conv layers to move  $\kappa_k$  from  $u_k$  to identity.  $\square$

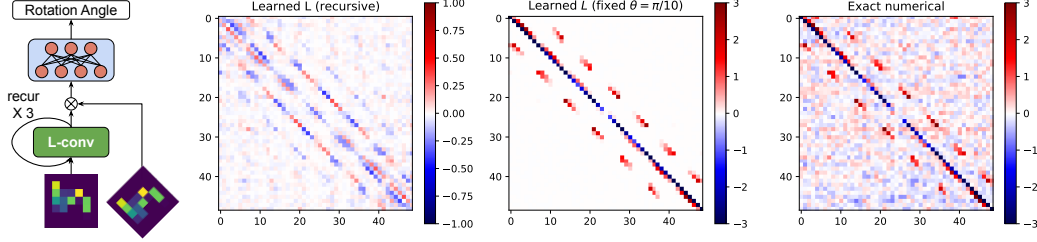


Figure 3: **Learning the infinitesimal generator of  $SO(2)$**  Left shows the architecture for learning rotation angles between pairs of images (SI C.3). Next to it is the  $L$  learned using recursive L-conv in this experiment. Middle  $L$  is learned using a fixed small rotation angle  $\theta = \pi/10$ , and right shows  $L$  found using the numeric solution from the data.

**Lemma 2** (Moving kernels to identity). *The local kernel  $\kappa_k$  can be moved near identity.*

*Proof:* The local kernels  $\kappa_k(g) = \delta_\eta(gu_k)$  are nonzero around  $u_k$ . An L-conv with  $W^0 = I$  performs  $G[\kappa_k \star f](g) = \kappa_k \star f(gv_\epsilon)$ , which moves the  $\kappa_k$  by  $v_\epsilon = (I + \bar{\epsilon}^i L_i)$  on  $G$ . Thus, by applying multiple L-conv layers we can find  $Q_p \circ \dots \circ Q_1 \circ \kappa_k \approx c_k \delta_\eta$ . This can always be done using a set of  $v_{\epsilon_a} = (I + \bar{\epsilon}_a^i L_i)$  such that  $u_k \approx \prod_{a=1}^p v_{\epsilon_a}$ . With  $\|\epsilon_a\| < \eta$ , the error in  $u_k$  is  $O(\eta^{p+1})$ .  $\square$

Thus, we conclude that any G-conv equation 3 can be approximated by multilayer L-conv. We conducted small controlled experiments to verify this (SI C). We briefly discuss them here.

**Learning symmetries using L-conv** Rao & Ruderman (1999) introduced a basic version of L-conv and showed that it can learn 1D translation and 2D rotation. The learned  $L_i$  for 1D translation reproduced finite translation well using  $(I + \epsilon L)^N$ , which is  $N$  recursive L-conv layers. Hence, their results prove that L-conv can be used to approximate CNN, as well as  $SO(2)$  G-conv. We discuss the details of L-conv approximating CNN below in sec. 5. We also conducted more complex experiments using recursive L-conv to learn large rotation angle between two images (SI C). Figure 3 shows the learned  $L$ . Left shows  $L \in so(2)$  learned using L-conv in 3 recursive layers to learn rotation angles between a pair of  $7 \times 7$  random images  $\mathbf{f}$  and  $R(\theta)\mathbf{f}$  with  $\theta \in [0, \pi/3)$ . Middle and right of Fig. 3 are experiments with fixed small rotation angle  $\theta = \pi/10$  (SI C.2). Middle is the  $L$  learned using L-conv and right is using the exact solution  $R = (YX^T)(X^T X)^{-1}$ . While the middle  $L$  is less noisy, it does not capture weights beyond first neighbors of each pixel. (also see SI C for a discussion on symmetry discovery literature.)

L-conv can potentially replace other equivariant layers in an architectures. We conducted limited experiments for this on small image datasets (SI D). L-conv allows one to look for potential symmetries in data which may have been scrambled or harbors hidden symmetries. Since many datasets such as images deal with discretized spaces, we first need to derive how L-conv acts on such data, discussed next.

## 4 Tensor notation

In many datasets, such as images,  $f(\mathbf{x})$  is not given as continuous function, but rather as a discrete array, with  $\mathcal{S} = \{\mathbf{x}_0, \dots, \mathbf{x}_{d-1}\}$  containing  $d$  points. Each  $\mathbf{x}_\mu$  represents a coordinate in higher dimensional space, e.g. on a  $10 \times 10$  image,  $\mathbf{x}_0$  is  $(x, y) = (0, 0)$  point and  $\mathbf{x}_{99}$  is  $(x, y) = (9, 9)$ .

**Feature maps and group action** In the tensor notation, we encode  $\mathbf{x}_\mu \in \mathcal{S}$  as the canonical basis (one-hot) vectors in  $\mathbf{x}_\mu \in \mathbb{R}^d$  with  $[\mathbf{x}_\mu]_\nu = \delta_{\mu\nu}$  (Kronecker delta), e.g.  $\mathbf{x}_0 = (1, 0, \dots, 0)$ . The features become  $\mathbf{f} \in \mathcal{F} = \mathbb{R}^d \otimes \mathbb{R}^m$ , meaning  $d \times m$  tensors, with  $f(\mathbf{x}_\mu) = \mathbf{x}_\mu^T \mathbf{f} = \mathbf{f}_\mu$ . Although  $\mathcal{S}$  is discrete, the group acting on  $\mathcal{F}$  can be continuous (e.g. image rotations). Any  $G \subseteq GL_d(\mathbb{R})$  of the general linear group (invertible  $d \times d$  matrices) acts on  $\mathbf{x}_\mu \in \mathbb{R}^d$  and  $\mathbf{f} \in \mathcal{F}$ . We define  $f(g \cdot \mathbf{x}_\mu) = \mathbf{x}_\mu^T g^T \mathbf{f}, \forall g \in G$ , so that for  $w \in G$  we have

$$w \cdot f(\mathbf{x}_\mu) = f(w^{-1} \cdot \mathbf{x}_\mu) = \mathbf{x}_\mu^T w^{-1T} \mathbf{f} = [w^{-1} \mathbf{x}_\mu]^T \mathbf{f} \quad (12)$$

Dropping the position  $\mathbf{x}_\mu$ , the transformed features are matrix product  $w \cdot \mathbf{f} = w^{-1T} \mathbf{f}$ .

**G-conv and L-conv in tensor notation** Writing G-conv equation 3 in the tensor notation we have

$$[\mathbf{f} \star \kappa](g\mathbf{x}_0) = \int_G \kappa(v) f(gv\mathbf{x}_0) dv = \mathbf{x}_0^T \int_G v^T g^T \mathbf{f} \kappa^T(v) dv \equiv \mathbf{x}_0^T [\mathbf{f} \star \kappa](g) \quad (13)$$

where we moved  $\kappa^T(v) \in \mathbb{R}^m \otimes \mathbb{R}^{m'}$  to the right of  $\mathbf{f}$  because it acts as a matrix on the output index of  $\mathbf{f}$ . The equivariance of equation 13 is readily checked with  $w \in G$

$$w \cdot [\mathbf{f} \star \kappa](g) = [\mathbf{f} \star \kappa](w^{-1}g) = \mathbf{x}_0^T \int_G v^T g^T w^{-1T} \mathbf{f} \kappa^T(v) dv = [(w \cdot \mathbf{f}) \star \kappa](g) \quad (14)$$

where we used  $[w^{-1}g]^T \mathbf{f} = g^T w^{-1T} \mathbf{f}$ . Similarly, we can rewrite L-conv equation 6 in the tensor notation. Defining  $v_\epsilon = I + \bar{\epsilon}^i L_i$

$$\begin{aligned} Q[\mathbf{f}](g) &= W^0 f(g(I + \bar{\epsilon}^i L_i)) = \mathbf{x}_0^T (I + \bar{\epsilon}^i L_i)^T g^T \mathbf{f} W^{0T} \\ &= (\mathbf{x} + \bar{\epsilon}^i [gL_i \mathbf{x}_0])^T \mathbf{f} W^{0T}. \end{aligned} \quad (15)$$

Here,  $\hat{L}_i = gL_i \mathbf{x}_0$  is exactly the tensor analogue of pushforward vector field  $\hat{L}_i$  in equation 8. We will make this analogy more precise below.

The equivariance of L-conv in tensor notation is again evident from the  $g^T \mathbf{f}$ , resulting in

$$Q[w \cdot \mathbf{f}](g) = \mathbf{x}_0^T v_\epsilon^T g^T w^{-1T} \mathbf{f} W^{0T} = Q[\mathbf{f}](w^{-1}g) = w \cdot Q[\mathbf{f}](g) \quad (16)$$

**Tensor L-conv layer implementation** In conclusion, the discrete space L-conv equation 15 can be rewritten using the global Lie algebra basis  $\hat{L}_i$

$$Q[\mathbf{f}] = (\mathbf{f} + \hat{L}_i \mathbf{f} \bar{\epsilon}^i) W^{0T}, \quad Q[\mathbf{f}]_\mu^a = \mathbf{f}_\mu^b [W^{0T}]_b^a + [\hat{L}_i]_\mu^\nu \mathbf{f}_\nu^c [W^i]_c^a \quad (17)$$

Where  $W^i = W^0 \bar{\epsilon}^i$ ,  $W^0 \in \mathbb{R}^{m_{in}} \otimes \mathbb{R}^{m_{out}}$  and  $\bar{\epsilon}^i \in \mathbb{R}^{m_{in}} \otimes \mathbb{R}^{m_{in}}$  are trainable weights. The  $\hat{L}_i$  can be either inserted as inductive bias or they can be learned to discover symmetries.

To implement L-conv we note that the structure of equation 17 is quite similar to a Graph Convolutional Network (GCN) (Kipf & Welling, 2016). For each  $i$ , the shared convolutional weights are  $\bar{\epsilon}^i W^{0T}$  and the aggregation function of the GCN, a function of the graph adjacency matrix, is  $\hat{L}_i$  in L-conv. Thus, L-conv can be implemented as GCN modules for each  $\hat{L}_i$ , plus a residual connection for the  $\mathbf{f} W^{0T}$  term. Figure 4 shows the schematic of the structure of such an L-conv layer. In this method of implementing L-conv we treated  $\hat{L}_i$  as general  $d \times d$  matrices. However, being vector fields generated by the Lie algebra,  $\hat{L}_i$  can have a more constrained structure which allows them to be encoded and learned using much fewer parameters than a  $d \times d$  matrix. Next, we discuss these constraints.

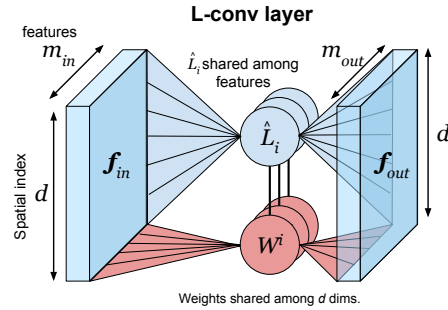


Figure 4: L-conv layer architecture.  $L_i$  only act on the  $d$  flattened spatial dimensions, and  $W^i$  only act on the  $m_{in}$  input features and returns  $m_{out}$  output features. For each  $i$ , L-conv is analogous to a Graph Convolutional Network with  $d$  nodes and  $m_{in}$  features.

**Discrete vector field and tangent bundle** We can

show (SI B.1) that when  $\mathcal{S}$  has a topology  $\hat{L}_i = gL_i \mathbf{x}_0$  is indeed the discrete version of the  $\hat{L}_i$  in equation 8. The topology, to lowest order, using a graph (1-simplex) is encoded as an incidence matrix  $\mathbf{B} : \mathcal{S} \times \mathcal{E} \rightarrow \{0, 1, -1\}$  with vertices  $\mathcal{S}$  and edge set  $\mathcal{E}$ .  $\mathbf{B}_\alpha^\mu = 1$  or  $-1$  if edge  $\alpha$  starts or ends at node  $\mu$ , respectively, and  $\mathbf{B}_\alpha^\mu = 0$  otherwise.  $\mathbf{B}$  is used to extend differential geometry to graphs (Schaub et al., 2020), since for  $\alpha$  an outgoing edge from vertex  $\mu$ , we have  $\mathbf{B}_\alpha \mathbf{f} = \mathbf{f}_\mu - \mathbf{f}_\nu \sim \partial_\alpha \mathbf{f}$ . We show that for  $G$  to preserve the topology, components of  $\hat{L}_i$  should act on the local neighborhood of each node and related to each other via the pushforward

$$[\hat{L}_i]_\mu^\nu = [g_\mu L_i \mathbf{x}_0]^\nu = [\hat{\ell}_i]_\mu^\alpha \mathbf{B}_\alpha^\nu = [\hat{\ell}_i]_0^\alpha \mathbf{B}_\alpha^\rho [g_\mu]_\rho^\nu. \quad (18)$$

$\hat{L}_i \equiv \hat{\ell}_i^\alpha \mathbf{B}_\alpha$  is the discrete  $\mathcal{S}$  version of the vector field  $\hat{L}_i(\mathbf{x}) = [gL_i\mathbf{x}_0]^\alpha \partial_\alpha$  in equation 8. Here  $[\hat{\ell}_i]_0^\alpha \in \mathbb{R}$  are weightings for edges  $\alpha$  connected to  $\mathbf{x}_0$  and capture the action of  $L_i$ . This weighting is similar to Gauge Equivariant Mesh (GEM) CNN (Cohen et al., 2019a). The main difference is that in GEM-CNN the basis of the tangent spaces  $T_{\mathbf{x}_\mu} \mathcal{S}$  are not fixed and are chosen by a gauge. In L-conv the lift  $\mathbf{x}_\mu = g_\mu \mathbf{x}_0$  fixes the gauge by mapping neighbors of  $\mathbf{x}_0$  to neighbors of  $\mathbf{x}_\mu$ . Changing how the discrete  $\mathcal{S}$  samples an underlying continuous space changes  $g_\mu$  and hence the gauge, similar to GEM-CNN. Next, we discuss the relation between L-conv and other neural architectures.

## 5 Relation to other architectures

L-conv can reproduce some familiar architectures for specific Lie groups, as we discuss now.

**CNN** This is a special case of expressing G-conv as L-conv when the group is continuous 1D translations. The arguments here generalize trivially to higher dimensions. Rao & Ruderman (1999, sec. 4) used the Shannon-Whittaker Interpolation (Whittaker, 1915) to define continuous translation on periodic 1D arrays as  $\mathbf{f}'_\rho = g(z)_\rho^\nu \mathbf{f}_\nu$ . Here  $g(z)_\rho^\nu = \frac{1}{d} \sum_{p=-d/2}^{d/2} \cos\left(\frac{2\pi p}{d}(z + \rho - \nu)\right)$  approximates the shift operator for continuous  $z$ . These  $g(z)$  form a 1D translation group  $G$  as  $g(w)g(z) = g(w+z)$  with  $g(0)_\rho^\nu = \delta_\rho^\nu$ . For any  $z = \mu \in \mathbb{Z}$ ,  $g_\mu = g(z = \mu)$  are circulant matrices that shift by  $\mu$  as  $[g_\mu]_\rho^\nu = \delta_{\nu-\mu}^\rho$ . Thus, a 1D CNN with kernel size  $k$  can be written using  $g_\mu$  as

$$F(\mathbf{f})_a^\nu = \sigma \left( \sum_{\mu=0}^k \mathbf{f}_{\nu-\mu}^c [W^\mu]_c^a + b^a \right) = \sigma \left( \sum_{\mu=0}^k [g_\mu \mathbf{f}]_\nu^c [W^\mu]_c^a + b^a \right) \quad (19)$$

where  $W, b$  are the filter weights and biases.  $g_\mu$  can be approximated using the Lie algebra and written as multi-layer L-conv as in sec. 3.2. Using  $g(0)_\rho^\nu \approx \delta(\rho - \nu)$ , the single Lie algebra basis  $[\hat{L}]_0 = \partial_z g(z)|_{z \rightarrow 0}$ , acts as  $\hat{L}f(z) \approx -\partial_z f(z)$  (because  $\int \partial_z \delta(z - \nu) f(z) = -\partial_\nu f(\nu)$ ). Its components are  $\hat{L}_\rho^\nu = L(\rho - \nu) = \sum_p \frac{2\pi p}{d^2} \sin\left(\frac{2\pi p}{d}(\rho - \nu)\right)$ , which are also circulant due to the  $(\rho - \nu)$  dependence. Hence,  $[\hat{L}\mathbf{f}]_\rho = \sum_\nu L(\rho - \nu) \mathbf{f}_\nu = [L \star \mathbf{f}]_\rho$  is a convolution. Rao & Ruderman (1999) already showed that this  $\hat{L}$  can reproduce finite discrete shifts  $g_\mu$  used in CNN. They used a primitive version of L-conv with  $g_\mu = (I + \epsilon \hat{L})^N$ . Thus, L-conv can approximate 1D CNN. This result generalizes easily to higher dimensions.

**Relation with Graph Convolutional Networks (GCN)** Let  $\mathbf{A}$  be the adjacency matrix of a graph. In equation 17 if  $\hat{L}_i = h(\mathbf{A})$ , such as  $\hat{L}_i = \mathbf{D}^{-1/2} \mathbf{A} \mathbf{D}^{-1/2}$ , we obtain a GCN (Kipf & Welling, 2016) ( $\mathbf{D}_{\mu\nu} = \delta_{\mu\nu} \sum_\rho \mathbf{A}_{\mu\rho}$  being the degree matrix). So in the special case where all neighbors of each node  $\langle \mu \rangle$  have the same edge weight, meaning  $[\hat{L}_i]_\mu^\nu = [\hat{L}_i]_\mu^\rho, \forall \nu, \rho \in \langle \mu \rangle$ , equation 6 is uniformly aggregating over neighbors and L-conv reduces to a GCN. Note that this similarity is not just superficial. In GCN  $h(\mathbf{A}) = \hat{L}$  is in fact a Lie algebra basis. When  $\hat{L} = h(\mathbf{A})$ , the vector field is the flow of isotropic diffusion  $d\mathbf{f}/dt = h(\mathbf{A})\mathbf{f}$  from each node to its neighbors. This vector field defines one parameter Lie group with elements  $g(t) = \exp[h(\mathbf{A})t]$ . Hence, L-conv for flow groups with a single generator are GCN. These flow groups include Hamiltonian flows and other linear dynamical systems.

The main difference between L-conv and GCN is that L-conv can assign a different weight to each neighbor of the same node. This weighting is similar to Gauge Equivariant Mesh (GEM) CNN (Cohen et al., 2019a). The main difference is that in GEM-CNN the basis of the tangent spaces  $\langle \mu \rangle = T_{\mathbf{x}_\mu} \mathcal{S}$  are not fixed and are chosen by a gauge. In L-conv the lift  $\mathbf{x}_\mu = g_\mu \mathbf{x}_0$  fixes the gauge, meaning it determines how the basis at  $\langle 0 \rangle$  maps to the basis at  $\langle \mu \rangle$ . Changing how the discrete  $(\mathcal{S}, \mathbf{A})$  samples the underlying topological space  $\mathcal{S}_0$  changes the lift  $g_\mu$  and hence the gauge, similar to GEM-CNN. Next, we discuss the mathematical properties of loss functions for L-conv.

## 6 Group invariant loss

Loss functions of equivariant architectures are rarely discussed. Yet, recent work by Kunin et al. (2020) showed existence of symmetry directions in the loss landscape. To understand how the

symmetry generators in L-conv manifest themselves in the loss landscape, we work out the explicit example of a mean square loss (MSE). Because  $G$  is the symmetry group,  $f$  and  $g \cdot f$  should result in the same optimal parameters. Hence, the minima of the loss function need to be *group invariant*. One way to satisfy this is for the loss itself to be group invariant, which can be constructed by integrating over  $G$  (global pooling (Bronstein et al., 2021)). A function  $I = \int_G dg F(g)$  is  $G$ -invariant (SI A.3). We can also change the integration to  $\int_S d^n x$  by change of variable  $dg/dx$  (see SI A.3 for discussion on stabilizers).

**MSE loss** The MSE is given by  $I = \sum_n \int_G dg \|Q[f_n](g)\|^2$ , where  $f_n$  are data samples and  $Q[f]$  is L-conv or another  $G$ -equivariant function. In supervised learning the input is a pair  $f_n, y_n$ .  $G$  can also act on the labels  $y_n$ . We assume that  $y_n$  are either also scalar features  $y_n : \mathcal{S} \rightarrow \mathbb{R}^{m_y}$  with a group action  $g \cdot y_n(\mathbf{x}) = y_n(g^{-1}\mathbf{x})$  (e.g.  $f_n$  and  $y_n$  are both images), or that  $y_n$  are categorical. In the latter case  $g \cdot y_n = y_n$  because the only representations of a continuous  $G$  on a discrete set are constant. We can concatenate the inputs to  $\phi_n \equiv [f_n | y_n]$  with a well-defined  $G$  action  $g \cdot \phi_n = [g \cdot f_n | g \cdot y_n]$ . The collection of combined inputs  $\Phi = (\phi_1, \dots, \phi_N)^T$  is an  $(m + m_y) \times N$  matrix. Using equations 6 and 8, the MSE loss with parameters  $W = \{W^0, \bar{\epsilon}\}$  becomes (SI A.3.1)

$$\begin{aligned} I[\Phi; W] &= \int_G dg \mathcal{L}[\Phi; W] = \int_G dg \left\| W^0 \left[ I + \bar{\epsilon}^i [\hat{L}_i]^\alpha \partial_\alpha \right] \Phi(g) \right\|^2 \\ &= \int_S \frac{d^n x}{\left| \frac{\partial x}{\partial g} \right|} \left[ \Phi^T \mathbf{m}_2 \Phi + \partial_\alpha \Phi^T \mathbf{h}^{\alpha\beta} \partial_\beta \Phi + [\hat{L}_i]^\alpha \partial_\alpha (\Phi^T \mathbf{v}^i \Phi) \right] \end{aligned} \quad (20)$$

where  $\left| \frac{\partial x}{\partial g} \right|$  is the determinant of the Jacobian,  $W^i = W^0 \bar{\epsilon}^i$  and

$$\mathbf{m}_2 = W^{0T} W^0, \quad \mathbf{h}^{\alpha\beta}(\mathbf{x}) = \bar{\epsilon}^{iT} \mathbf{m}_2 \bar{\epsilon}^j [\hat{L}_i]^\alpha [\hat{L}_j]^\beta, \quad \mathbf{v}^i = \mathbf{m}_2 \bar{\epsilon}^i. \quad (21)$$

Note that  $\mathbf{h}$  has feature space indices via  $[\bar{\epsilon}^{iT} \mathbf{m}_2 \bar{\epsilon}^j]_{ab}$ , with index symmetry  $\mathbf{h}_{ab}^{\alpha\beta} = \mathbf{h}_{ba}^{\beta\alpha}$ . When  $\mathcal{F} = \mathbb{R}$  (i.e.  $f$  is a 1D scalar),  $\mathbf{h}^{\alpha\beta}$  becomes a Riemannian metric for  $\mathcal{S}$ . In general  $\mathbf{h}$  combines a 2-tensor  $\mathbf{h}_{ab} = \mathbf{h}_{ab}^{\alpha\beta} \partial_\alpha \partial_\beta \in TS \otimes TS$  with an inner product  $h^T \mathbf{h}^{\alpha\beta} f$  on the feature space  $\mathcal{F}$ . Hence  $\mathbf{h} \in TS \otimes TS \otimes \mathcal{F}^* \otimes \mathcal{F}^*$  is a  $(2, 2)$ -tensor, with  $\mathcal{F}^*$  being the dual space of  $\mathcal{F}$ .

A simpler version of the loss function in equation 20 is commonly used in field theories in physics (Polyakov, 2018). There too, the motivation is to preserve spatial symmetries for the metric  $\mathbf{h}$ . In equation 20,  $\mathbf{h}$  transforms equivariantly as a 2-tensor  $v \cdot \mathbf{h}^{\alpha\beta} = [v^{-1}]_\rho^\alpha [v^{-1}]_\sigma^\beta \mathbf{h}^{\rho\sigma}(\mathbf{x})$  for  $v \in G$  (SI A.3). In physics the last term in equation 20 is absent. We can show that for L-conv also when  $G$  is translations  $T_n$ , or rotations  $SO(n)$ , by partial integration the last term becomes a boundary term and expected to vanish (SI A.3). We discuss the implications of this overlap between physics and equivariant neural networks further below. One aspect of the physics theory which may benefit machine learning is that for  $\phi_n$  which minimize the loss, the loss function is robust to small perturbations. This yields a natural way to probe generalization in equivariant neural networks, discussed next.

**Generalization error** Equivariant neural networks are expected to be more robust than others, meaning equivariance should improve generalization. One way to check this is to see how the network would perform for an input  $\phi' = \phi + \delta\phi$  which adds a small perturbation  $\delta\phi$  to a real data point  $\phi$ . Note  $\delta\phi$  here is a random noise, not an adversarial attack. Robustness to such perturbation would mean that, for optimal parameters  $W^*$ , the loss function would not change, i.e.  $I[\phi'; W^*] = I[\phi; W^*]$ . This can be cast as a variational equation, requiring  $I$  to be minimized around real data points  $\phi$ . Writing  $I[\phi; W] = \int d^n x \mathcal{L}[\phi; W]$ , we have

$$\delta I[\phi; W^*] = \int_S d^n x \left[ \frac{\partial \mathcal{L}}{\partial \phi^a} \delta \phi^a + \frac{\partial \mathcal{L}}{\partial (\partial_\alpha \phi^a)} \partial_\alpha (\delta \phi^a) \right] \quad (22)$$

Doing a partial integration on the second term, we get a vanishing boundary term plus the familiar Euler-Lagrange (EL) equation (SI A.4), widely used in physics and control theory. Thus, requiring good generalization, i.e.  $\delta I[\phi; W^*]/\delta\phi = 0$  means for optimal parameters  $W^*$ , real data points  $\phi$  satisfy the EL equations

$$\text{Generalization Error Minimization} \iff \text{EL: } \frac{\partial \mathcal{L}}{\partial \phi^b} - \partial_\alpha \frac{\partial \mathcal{L}}{\partial (\partial_\alpha \phi^b)} = 0 \quad (23)$$

Another idea which can be transferred from physics to equivariant neural networks is that symmetries produce conserved currents, via Noether’s theorem, also discussed in Kunin et al. (2020). We briefly discuss motivate this below.

**Conservation laws** The idea is that the equivariance condition equation 2 can be written for the integrand of the loss  $\mathcal{L}[\phi, W]$ . If we write the equivariance equation for infinitesimal  $v_\epsilon$ , we obtain a vector field which is divergence free. Since  $G$  is the symmetry of the system, transforming an input  $\phi \rightarrow w \cdot \phi$  by  $w \in G$  the integrand should change equivariantly, meaning  $\mathcal{L}[w \cdot \phi] = w \cdot \mathcal{L}[\phi]$ . When generalization error is minimized as in equation 23, an infinitesimal  $w \approx I + \eta^i L_i$ , with  $\delta\phi = \epsilon^i \hat{L}_i \phi$ , results in a conserved current (SI A.4)

$$\text{Noether current: } J^\alpha = \frac{\partial \mathcal{L}}{\partial(\partial_\alpha \phi^b)} \delta\phi^b - \frac{\partial \mathcal{L}}{\partial x^\alpha} \delta x^\alpha, \quad \delta I[\phi; W^*] = 0 \Rightarrow \partial_\alpha J^\alpha = 0 \quad (24)$$

This  $J$  is called the Noether current in physics. It captures the flow of the Lagrangian  $\mathcal{L}$  along symmetry direction  $\hat{L}_i$ . It would be interesting to see if these conserved currents can be used in practice as an alternative way for identifying or discovering symmetries. We conclude by remarking on similarity between ML and physics problems.

**Relation to physics** Although equation 20 was derived purely using ML and equivariance, physicists will recognize equation 20 as a generalization of the non-interacting field theory action (integral of a Lagrangian). In field theory,  $\phi(x)$  (each input feature  $[f|y]$ ) is called a field.  $\mathbf{m}_2$  is the “mass matrix” whose eigenvalues are the squares of masses of the fields. The second term  $\partial\phi^T \cdot \mathbf{h} \cdot \partial\phi = \partial^\mu \phi^\alpha \partial_\mu \phi_\alpha$  is the “kinetic” term. In physics, the loss in equation 20 is used in two ways. When the parameters  $\mathbf{m}_2$  and  $\mathbf{h}$  are known, a variational procedure known as the Euler-Lagrange equations is used to find optimal  $\phi(x) = \arg \min_\phi I[\phi]$ . When  $\mathbf{m}_2$  and  $\mathbf{h}$  are not known,  $\phi_n$  are observational data and physicists use equation 20 the same way as ML. In this case equation 20 is a variational ansatz used to identify parameters  $\mathbf{m}_2$  and  $\mathbf{h}$  such that the expected loss for the observed  $\phi_n$  is minimized. The main difference with physics is that physics assumes a simpler form in which  $\mathbf{h}$  factorizes into a tensor product  $\mathbf{h} = \eta \otimes \delta$ , where  $\eta_{\alpha\beta}$  is a Riemannian metric on  $\mathcal{T}\mathcal{S}$  and  $\delta$ , usually the Kronecker delta, is the metric on  $\mathcal{F}$ . We conclude with some closing remarks.

## 7 Discussions

In conclusion, we found that expanding group convolutional architectures into a smaller building block, L-conv, has a number of benefits. First, L-conv has a much simpler and more familiar structure than G-conv. We showed that L-conv layers can be combined to approximate any G-conv, without the need to encode many irreps or discretizing the group. Additionally, L-conv’s simple structure allows us to discover symmetries from data. L-conv is easy to implement and can be implemented like a GCN. But perhaps the most interesting discovery here is the connection made with symmetry encoding models in physics. This is significant for two reasons. One is that methods for dealing with symmetry used in physics acquire important meanings in ML, as our discussion on the loss function, generalization and conservation laws show. The second reason is for scientific machine learning. Physicists usually use the simplest forms for the loss function, similar to the MSE loss above. Many areas of physics suffer from this because these ansatze diverge in many cases or fit the data poorly. Hence, more complex L-conv loss functions can potentially serve as more advanced ansatze for solving physics problems.

## Acknowledgments and Disclosure of Funding

### References

- Anselmi, F., Evangelopoulos, G., Rosasco, L., and Poggio, T. Symmetry-adapted representation learning. *Pattern Recognition*, 86:201–208, 2019.
- Belavin, A. A., Polyakov, A. M., and Zamolodchikov, A. B. Infinite conformal symmetry in two-dimensional quantum field theory. *Nuclear Physics B*, 241(2):333–380, 1984.
- Benton, G., Finzi, M., Izmailov, P., and Wilson, A. G. Learning invariances in neural networks. *arXiv preprint arXiv:2010.11882*, 2020.

- Bogatskiy, A., Anderson, B., Offermann, J., Roussi, M., Miller, D., and Kondor, R. Lorentz group equivariant neural network for particle physics. In *International Conference on Machine Learning*, pp. 992–1002. PMLR, 2020.
- Bronstein, M. M., Bruna, J., Cohen, T., and Velicković, P. Geometric deep learning: Grids, groups, graphs, geodesics, and gauges. *arXiv preprint arXiv:2104.13478*, 2021.
- Cohen, T. and Welling, M. Learning the irreducible representations of commutative lie groups. In *International Conference on Machine Learning*, pp. 1755–1763, 2014.
- Cohen, T. and Welling, M. Group equivariant convolutional networks. In *International conference on machine learning*, pp. 2990–2999, 2016a.
- Cohen, T., Weiler, M., Kicanaoglu, B., and Welling, M. Gauge equivariant convolutional networks and the icosahedral cnn. In *International Conference on Machine Learning*, pp. 1321–1330. PMLR, 2019a.
- Cohen, T. S. and Welling, M. Steerable cnns. 2016b.
- Cohen, T. S., Geiger, M., Köhler, J., and Welling, M. Spherical cnns. In *International Conference on Learning Representations*, 2018.
- Cohen, T. S., Geiger, M., and Weiler, M. A general theory of equivariant cnns on homogeneous spaces. In *Advances in Neural Information Processing Systems*, pp. 9142–9153, 2019b.
- Cybenko, G. Approximation by superpositions of a sigmoidal function. *Mathematics of control, signals and systems*, 2(4):303–314, 1989.
- Finzi, M., Stanton, S., Izmailov, P., and Wilson, A. G. Generalizing convolutional neural networks for equivariance to lie groups on arbitrary continuous data. *arXiv preprint arXiv:2002.12880*, 2020.
- Finzi, M., Welling, M., and Wilson, A. G. A practical method for constructing equivariant multilayer perceptrons for arbitrary matrix groups. *arXiv preprint arXiv:2104.09459*, 2021.
- Gilmer, J., Schoenholz, S. S., Riley, P. F., Vinyals, O., and Dahl, G. E. Neural message passing for quantum chemistry. In *International Conference on Machine Learning*, pp. 1263–1272. PMLR, 2017.
- Hall, B. *Lie groups, Lie algebras, and representations: an elementary introduction*, volume 222. Springer, 2015.
- Hartford, J., Graham, D., Leyton-Brown, K., and Ravanbakhsh, S. Deep models of interactions across sets. In *International Conference on Machine Learning*, pp. 1909–1918. PMLR, 2018.
- Hornik, K., Stinchcombe, M., and White, H. Multilayer feedforward networks are universal approximators. *Neural networks*, 2(5):359–366, 1989.
- Kipf, T. N. and Welling, M. Semi-supervised classification with graph convolutional networks. *arXiv preprint arXiv:1609.02907*, 2016.
- Kondor, R. and Trivedi, S. On the generalization of equivariance and convolution in neural networks to the action of compact groups. *arXiv preprint arXiv:1802.03690*, 2018.
- Kondor, R., Lin, Z., and Trivedi, S. Clebsch–gordan nets: a fully fourier space spherical convolutional neural network. In *Advances in Neural Information Processing Systems*, pp. 10117–10126, 2018.
- Kunin, D., Sagastuy-Brena, J., Ganguli, S., Yamins, D. L., and Tanaka, H. Neural mechanics: Symmetry and broken conservation laws in deep learning dynamics. *arXiv preprint arXiv:2012.04728*, 2020.
- Landau, L. D. *The classical theory of fields*, volume 2. Elsevier, 2013.
- LeCun, Y., Boser, B., Denker, J. S., Henderson, D., Howard, R. E., Hubbard, W., and Jackel, L. D. Backpropagation applied to handwritten zip code recognition. *Neural computation*, 1(4):541–551, 1989.

- LeCun, Y., Bottou, L., Bengio, Y., and Haffner, P. Gradient-based learning applied to document recognition. *Proceedings of the IEEE*, 86(11):2278–2324, 1998.
- Lee, J. M., Chow, B., Chu, S.-C., Glickenstein, D., Guenther, C., Isenberg, J., Ivey, T., Knopf, D., Lu, P., Luo, F., et al. Manifolds and differential geometry. *Topology*, 643:658, 2009.
- Maron, H., Litany, O., Chechik, G., and Fetaya, E. On learning sets of symmetric elements. In *International Conference on Machine Learning*, pp. 6734–6744. PMLR, 2020.
- Polyakov, A. M. *Gauge fields and strings*. Routledge, 2018.
- Rao, R. P. and Ruderman, D. L. Learning lie groups for invariant visual perception. In *Advances in neural information processing systems*, pp. 810–816, 1999.
- Ravanbakhsh, S. Universal equivariant multilayer perceptrons. *arXiv preprint arXiv:2002.02912*, 2020.
- Ravanbakhsh, S., Schneider, J., and Póczos, B. Equivariance through parameter-sharing. In *Proceedings of the 34th International Conference on Machine Learning-Volume 70*, pp. 2892–2901. JMLR.org, 2017.
- Schaub, M. T., Benson, A. R., Horn, P., Lippner, G., and Jadbabaie, A. Random walks on simplicial complexes and the normalized hodge 1-laplacian. *SIAM Review*, 62(2):353–391, 2020.
- Sohl-Dickstein, J., Wang, C. M., and Olshausen, B. A. An unsupervised algorithm for learning lie group transformations. *arXiv preprint arXiv:1001.1027*, 2010.
- Weiler, M. and Cesa, G. General e (2)-equivariant steerable cnns. In *Advances in Neural Information Processing Systems*, pp. 14334–14345, 2019.
- Weiler, M., Geiger, M., Welling, M., Boomsma, W., and Cohen, T. S. 3d steerable cnns: Learning rotationally equivariant features in volumetric data. In *Advances in Neural Information Processing Systems*, pp. 10381–10392, 2018a.
- Weiler, M., Hamprecht, F. A., and Storath, M. Learning steerable filters for rotation equivariant cnns. In *Proceedings of the IEEE Conference on Computer Vision and Pattern Recognition*, pp. 849–858, 2018b.
- Weinberg, S. *The quantum theory of fields*, volume 3. Cambridge university press, 1995.
- Whitaker, E. On the functions which are represented by the expansion of interpolating theory. In *Proc. Roy. Soc. Edinburgh*, volume 35, pp. 181–194, 1915.
- Worrall, D. E., Garbin, S. J., Turmukhambetov, D., and Brostow, G. J. Harmonic networks: Deep translation and rotation equivariance. In *Proceedings of the IEEE Conference on Computer Vision and Pattern Recognition*, pp. 5028–5037, 2017.
- Zaheer, M., Kottur, S., Ravanbakhsh, S., Póczos, B., Salakhutdinov, R. R., and Smola, A. J. Deep sets. In *Advances in neural information processing systems*, pp. 3391–3401, 2017.
- Zhou, A., Knowles, T., and Finn, C. Meta-learning symmetries by reparameterization. *arXiv preprint arXiv:2007.02933*, 2020.

## Checklist

The checklist follows the references. Please read the checklist guidelines carefully for information on how to answer these questions. For each question, change the default **[TODO]** to **[Yes]**, **[No]**, or **[N/A]**. You are strongly encouraged to include a **justification to your answer**, either by referencing the appropriate section of your paper or providing a brief inline description. For example:

- Did you include the license to the code and datasets? **[Yes]** See Section
- Did you include the license to the code and datasets? **[No]** The code and the data are proprietary.

- Did you include the license to the code and datasets? [N/A]

Please do not modify the questions and only use the provided macros for your answers. Note that the Checklist section does not count towards the page limit. In your paper, please delete this instructions block and only keep the Checklist section heading above along with the questions/answers below.

1. For all authors...
  - (a) Do the main claims made in the abstract and introduction accurately reflect the paper's contributions and scope? [Yes]
  - (b) Did you describe the limitations of your work? [No]
  - (c) Did you discuss any potential negative societal impacts of your work? [N/A]
  - (d) Have you read the ethics review guidelines and ensured that your paper conforms to them? [Yes]
2. If you are including theoretical results...
  - (a) Did you state the full set of assumptions of all theoretical results? [Yes]
  - (b) Did you include complete proofs of all theoretical results? [Yes]
3. If you ran experiments...
  - (a) Did you include the code, data, and instructions needed to reproduce the main experimental results (either in the supplemental material or as a URL)? [Yes]
  - (b) Did you specify all the training details (e.g., data splits, hyperparameters, how they were chosen)? [Yes]
  - (c) Did you report error bars (e.g., with respect to the random seed after running experiments multiple times)? [Yes]
  - (d) Did you include the total amount of compute and the type of resources used (e.g., type of GPUs, internal cluster, or cloud provider)? [Yes]
4. If you are using existing assets (e.g., code, data, models) or curating/releasing new assets...
  - (a) If your work uses existing assets, did you cite the creators? [Yes]
  - (b) Did you mention the license of the assets? [N/A]
  - (c) Did you include any new assets either in the supplemental material or as a URL? [Yes]
  - (d) Did you discuss whether and how consent was obtained from people whose data you're using/curating? [N/A]
  - (e) Did you discuss whether the data you are using/curating contains personally identifiable information or offensive content? [N/A]
5. If you used crowdsourcing or conducted research with human subjects...
  - (a) Did you include the full text of instructions given to participants and screenshots, if applicable? [N/A]
  - (b) Did you describe any potential participant risks, with links to Institutional Review Board (IRB) approvals, if applicable? [N/A]
  - (c) Did you include the estimated hourly wage paid to participants and the total amount spent on participant compensation? [N/A]

## A Extended derivations and proofs

**Path-ordered Exponential** Every element  $g \in G$  can be written as a product  $g = \prod_a \exp[t_a^i L_i]$  using the matrix exponential (Hall, 2015). This can be done using a path  $\gamma$  connecting  $I$  to  $g$  on the manifold of  $G$ . Here,  $t_a$  will be segments of the path  $\gamma$  which add up as vectors to connect  $I$  to  $g$ . This surjective map can be written as a ‘‘path-ordered’’ (or time-ordered in physics (Weinberg, 1995)) exponential (POE). In the simplest form, POE can be defined by breaking  $u = \prod_a \exp[t_a^i L_i]$  down into infinitesimal steps of size  $t_a = 1/N$  with  $N \rightarrow \infty$ . Choosing  $\gamma$  to be a differentiable path, we can replace the sum over segments  $\sum_a t_a$  with an integral along the path  $\sum_a t_a = \int_\gamma dt(s) ds$ , where  $t(s) = d\gamma/ds$  is the tangent vector to the path  $\gamma$ , where  $s \in [0, 1]$  parametrizes  $\gamma$ . The POE is then defined as the infinitesimal  $t_a$  limit of  $g = \prod_a \exp[t_a^i L_i]$ . This can be written as

$$\begin{aligned} g &= P \exp \left[ \int_\gamma t^i(s) L_i ds \right] = \lim_{N \rightarrow \infty} \prod_{a=1}^N \left( I + \delta s \gamma'^i(s_a) L_i \right) \\ &= \int_0^{s_1} ds_0 \gamma'^i(s_0) L_i \int_0^{s_2} ds_1 \gamma'^j(s_1) L_j \cdots \int_0^1 ds_N \gamma'^k(s_N) L_k \end{aligned} \quad (25)$$

**L-conv derivation** Let us consider what happens if the kernel in G-conv equation 3 is localized near identity. Let  $\kappa_I(u) = c \delta_\eta(u)$ , with constants  $c \in \mathbb{R}^{m'} \otimes \mathbb{R}^m$  and kernel  $\delta_\eta(u) \in \mathbb{R}$  which has support only on an  $\eta$  neighborhood of identity, meaning  $\delta_\eta(I + \epsilon^i L_i) \rightarrow 0$  if  $|\epsilon| > \eta$ . This allows us to expand G-conv in the Lie algebra of  $G$  to linear order. With  $v_\epsilon = I + \epsilon^i L_i$ , we have

$$\begin{aligned} [\delta_\eta \star f](g) &= \int_G dv \delta_\eta(v) f(gv) = \int_{\|\epsilon\| < \eta} dv_\epsilon \delta_\eta(v_\epsilon) f(gv_\epsilon) \\ &= \int d\epsilon \delta_\eta(I + \epsilon^i L_i) f(g(I + \epsilon^i L_i)) \\ &= \int d\epsilon \delta_\eta(I + \epsilon^i L_i) f(g + \epsilon^i g L_i) \\ &= \int d\epsilon \delta_\eta(I + \epsilon^i L_i) \left[ f(g) + \epsilon^i g L_i \cdot \frac{d}{dg} f(g) + O(\epsilon^2) \right] \\ &= \int d\epsilon \delta_\eta(I + \epsilon^i L_i) \left[ I + \epsilon^i g L_i \cdot \frac{d}{dg} \right] f(g) + O(\eta^2) \\ &= W^0 \left[ I + \bar{\epsilon}^i g L_i \cdot \frac{d}{dg} \right] f(g) + O(\eta^2) \end{aligned} \quad (26)$$

where  $d\epsilon$  is the integration measure on the Lie algebra induced by the Haar measure  $dv$  on  $G$ . The  $O(\eta^2)$  term arises from integrating the  $O(\epsilon^2)$  terms. To see this, note that for an order  $p$  function  $\phi(\epsilon)$ , for  $|\epsilon| < \eta$ ,  $|\phi(\epsilon)| < \eta^p C$  (for some constant  $C$ ). Substituting this bound into the integral over the kernel  $\delta_\eta$  we get

$$\begin{aligned} \left| \int d\epsilon \delta_\eta(I + \epsilon^i L_i) \phi(\epsilon) \right| &\leq \int |d\epsilon \delta_\eta(I + \epsilon^i L_i) \phi(\epsilon)| \\ &< \int |d\epsilon \delta_\eta(I + \epsilon^i L_i) \eta^p C| \leq \eta^p C \int |d\epsilon \delta_\eta(I + \epsilon^i L_i)| \leq \eta^p C \end{aligned} \quad (27)$$

In matrix representations,  $g L_i \cdot \frac{df}{dg} = [g L_i]_\alpha^\beta \frac{df}{dg^\beta} = \text{Tr} \left[ [g L_i]^T \frac{df}{dg} \right]$ . Note that in  $g(I + \epsilon^i L_i) \mathbf{x}_0$ , the  $g L_i \mathbf{x}_0 = \hat{L}_i(g) \mathbf{x}$  come from the pushforward  $\hat{L}_i(g) = g L_i g^{-1} \in T_g G$ . Here

$$W^0 = c \int d\epsilon \delta_\eta(I + \epsilon^i L_i) \in \mathbb{R}^{m'} \otimes \mathbb{R}^m, \quad \bar{\epsilon}^i = \frac{\int d\epsilon \delta_\eta(I + \epsilon^i L_i) \epsilon^i}{\int d\epsilon \delta_\eta(I + \epsilon^i L_i)} \in \mathbb{R}^m \otimes \mathbb{R}^m \quad (28)$$

with  $\|\bar{\epsilon}\| < \eta$ . When  $\delta_\eta$  is normalized, meaning  $\int_G \delta_\eta(g) dg = 1$ , we have  $W^0 = c$  and

$$\bar{\epsilon}^i = \int d\epsilon \delta_\eta(I + \epsilon^i L_i) \epsilon^i$$

Note that with  $f(g) \in \mathbb{R}^m$ , each  $\epsilon^i \in \mathbb{R}^m \otimes \mathbb{R}^m$  is a matrix. With indices,  $f(gv_\epsilon)$  is given by

$$[f(gv_\epsilon)]^a = \sum_b f^b(g(\delta_b^a + [\epsilon^i]_b^a L_i)) \quad (29)$$

Similarly, the integration measure  $d\epsilon$ , which is induced by the Haar measure  $dv_\epsilon \equiv d\mu(v_\epsilon)$ , is a product  $\int d\epsilon = \int |J| \prod [d[\epsilon^i]_b^a]$ , with  $J = \partial v_\epsilon / \partial \epsilon$  being the Jacobian.

Equation 26 is the core of the architecture we are proposing, the Lie algebra convolution or **L-conv**.

**L-conv Layer** In general, we define Lie algebra convolution (L-conv) as follows

$$\begin{aligned} Q[f](g) &= W^0 \left[ I + \bar{\epsilon}^i g L_i \cdot \frac{d}{dg} \right] f(g) \\ &= [W^0]_b f^a (g (\delta_a^b + [\bar{\epsilon}^i]_a^b L_i)) + O(\bar{\epsilon}^2) \end{aligned} \quad (30)$$

**Extended equivariance for L-conv** From equation 30 we see that  $W^0$  acts on the output feature indices. Notice that the equivariance of L-conv is due to the way  $gv_\epsilon = g(I + \bar{\epsilon}^i L_i)$  appears in the argument, since for  $u \in G$

$$u \cdot Q[f](g) = W^0 f(u^{-1} gv_\epsilon) = W^0 [u \cdot f](gv_\epsilon) \quad (31)$$

Because of this, replacing  $W^0$  with a general neural network which acts on the feature indices separately will not affect equivariance. For instance, if we pass L-conv through a neural network to obtain a generalized L-conv  $Q_\sigma$ , we have

$$\begin{aligned} Q_\sigma[f](g) &= \sigma(Wf(gv_\epsilon) + b) \\ u \cdot Q_\sigma[f](g) &= Q_\sigma[f](u^{-1}g) = \sigma(Wf(u^{-1}gv_\epsilon) + b) \\ &= \sigma(W[u \cdot f](gv_\epsilon) + b) = Q_\sigma[u \cdot f](g) \end{aligned} \quad (32)$$

Thus, L-conv can be followed by any nonlinear neural network as long as it only acts on the feature indices (i.e.  $a$  in  $f^a(g)$ ) and not on the spatial indices  $g$  in  $f(g)$ .

### A.1 Approximating G-conv using L-conv

We now show that G-conv equation 3 can be approximated by composing L-conv layers.

**Universal approximation for kernels** Using the same argument used for neural networks (Hornik et al., 1989; Cybenko, 1989), we may approximate any kernel  $\kappa(v)$  as the sum of a number of kernels  $\kappa_k$  with support only on a small  $\eta$  neighborhood of  $u_k \in G$  to arbitrary accuracy. The local kernels can be written as  $\kappa_k(v) = c_k \delta_\eta(u_k^{-1}v)$ , with  $\delta_\eta(u)$  as in equation 26 and constants  $c_k \in \mathbb{R}^{m'} \otimes \mathbb{R}^m$ . Using this, G-conv equation 3 becomes

$$\begin{aligned} [\kappa \star f](g) &= \sum_k [\kappa_k \star f](g) = \sum_k c_k \int dv \delta_\eta(u_k^{-1}v) f(gv) \\ &= \sum_k c_k \int dv \delta_\eta(v) f(gu_k v) = \sum_k c_k [\delta_\eta \star f](gu_k). \end{aligned} \quad (33)$$

As we showed in equation 26,  $[\delta_\eta \star f](g)$  is the definition of L-conv. Next, we need to show that  $[\delta_\eta \star f](gu_k)$  can also be approximated with  $[\delta_\eta \star f](g)$  and hence L-conv. For this we use  $u_k = v_k(I + \epsilon_k^i L_i)$  to find  $v_k \in G$  which are closer to  $I$  than  $u_k$ . Taylor expanding  $F_\eta = \delta_\eta \star f$  in  $\epsilon$  we obtain

$$\begin{aligned} F_\eta(gu_k) &= F_\eta(gv_k(I + \epsilon_k^i L_i)) = F_\eta(gv_k) + \epsilon_k^i u L_i \cdot \frac{dF_\eta(u)}{du} \Big|_{u \rightarrow gv_k} + O(\epsilon^2) \\ [\kappa \star f](g) &= \sum_k c_k F_\eta(gu_k) = \sum_k \left[ c_k + c_k \epsilon_k^i u L_i \cdot \frac{d}{du} \right] F_\eta(u) \Big|_{u \rightarrow gv_k} \\ &= \sum_k \left[ W_k^0 + W_k^i u L_i \cdot \frac{d}{du} \right] F_\eta(u) \Big|_{u \rightarrow gv_k} = \sum_k Q_k[F_\eta](gv_k) \end{aligned} \quad (34)$$

Using equation 34 we can progressively remove the  $u_k$  as  $F_\eta(gu_k) \approx Q_k^n[\dots[Q_k^1[F_\eta]]](g)$ , i.e. an  $n$  layer L-conv. Thus, we conclude that any G-conv equation 3 can be approximated by multilayer L-conv.

## A.2 Example of continuous L-conv

The  $gL_i \cdot df/dg$  in equation 6 can be written in terms of partial derivatives  $\partial_\alpha f(\mathbf{x}) = \partial f / \partial \mathbf{x}^\alpha$ . In general, using  $\mathbf{x}^\rho = g_\rho^\sigma \mathbf{x}_0^\sigma$ , we have

$$\frac{df(g\mathbf{x}_0)}{dg_\beta^\alpha} = \frac{d(g_\sigma^\rho \mathbf{x}_0^\sigma)}{dg_\beta^\alpha} \partial_\rho f(\mathbf{x}) = \mathbf{x}_0^\beta \partial_\alpha f(\mathbf{x}) \quad (35)$$

$$gL_i \cdot \frac{df}{dg} = [gL_i]_\beta^\alpha \mathbf{x}_0^\beta \partial_\alpha f(\mathbf{x}) = [gL_i \mathbf{x}_0] \cdot \nabla f(\mathbf{x}) = \hat{L}_i f(\mathbf{x}) \quad (36)$$

Hence, for each  $L_i$ , the pushforward  $gL_i$  generates a flow on  $\mathcal{S}$  through the vector field  $\hat{L}_i \equiv gL_i \cdot d/dg = [gL_i \mathbf{x}_0]^\alpha \partial_\alpha$  (Fig. 1). Being a vector field  $\hat{L}_i \in TS$  (i.e. 1-tensor),  $\hat{L}_i$  is basis independent, meaning for  $v \in G$ ,  $\hat{L}_i(v\mathbf{x}) = \hat{L}_i$ . Its components transform as  $[\hat{L}_i(v\mathbf{x})]^\alpha = [v gL_i \mathbf{x}_0]^\alpha = v_\beta^\alpha \hat{L}_i(\mathbf{x})^\beta$ , while the partial transforms as  $\partial / \partial [v\mathbf{x}]^\alpha = [v^{-1}]_\alpha^\gamma \partial_\gamma$ . Using this relation and Taylor expanding equation 10, we obtain a second form for the group action on L-conv. For  $w \in G$ , with  $\mathbf{y} = w^{-1}\mathbf{x}$  we have

$$Q[f](w^{-1}g\mathbf{x}_0) = W^0 \left[ I + \bar{\epsilon}^i [\hat{L}_i]^\alpha [w^{-1}]_\alpha^\beta \frac{\partial}{\partial \mathbf{y}^\beta} \right] f(\mathbf{y}) \Big|_{\mathbf{y} \rightarrow w^{-1}\mathbf{x}} \quad (37)$$

**1D Translation:** Let  $G = T_1 = (\mathbb{R}, +)$ . A matrix representation for  $G$  is found by encoding  $x$  as a 2D vector  $(x, 1)$ . The lift is given by  $\mathbf{x}_0 = (0, 1)$  as the origin and  $g = \begin{pmatrix} 1 & x \\ 0 & 1 \end{pmatrix}$ . The

Lie algebra basis is  $L = \begin{pmatrix} 0 & 1 \\ 0 & 0 \end{pmatrix}$ . It is easy to check that  $gg'\mathbf{x}_0 = (x + x', 1)$ . We also find  $gL = L$ , meaning  $L$  looks the same in all  $T_g G$ . Close to identity  $I = 0$ ,  $v_\epsilon = I + \epsilon L = \epsilon$ . We have  $gv_\epsilon \mathbf{x}_0 = (g + \epsilon gL)\mathbf{x}_0 = (x + \epsilon, 1)$ . Thus,  $f(g(I + \epsilon L)\mathbf{x}_0) \approx f(\mathbf{x}) + \epsilon df(\mathbf{x})/d\mathbf{x}$ . This readily generalizes to  $n$ D translations  $T_n$  (SI A.2.2), yielding  $f(\mathbf{x}) + \epsilon^\alpha \partial_\alpha f(\mathbf{x})$ .

**2D Rotation:** Let  $G = SO(2)$ . The space which  $SO(2)$  can lift is not the full  $\mathbb{R}^2$ , but a circle of fixed radius  $r = \sqrt{x^2 + y^2}$ . Hence we choose  $\mathcal{S} = S^1$  embedded in  $\mathbb{R}^2$ , with  $x = r \cos \theta$  and  $y = r \sin \theta$ . For the lift, we use the standard 2D representation. We have  $\mathbf{x}_0 = (r, 0)$  and (see SI A.2.1)

$$L = \begin{pmatrix} 0 & -1 \\ 1 & 0 \end{pmatrix}, \quad g = \exp[\theta L] = \frac{1}{r} \begin{pmatrix} x & -y \\ y & x \end{pmatrix}, \quad gL \cdot \frac{df}{dg} = (x\partial_y - y\partial_x) f. \quad (38)$$

Physicists will recognize  $\hat{L} \equiv (x\partial_y - y\partial_x) = \partial_\theta$  as the angular momentum operator in quantum mechanics and field theories, which generates rotations around the  $z$  axis.

**Rotation and scaling** Let  $G = SO(2) \times \mathbb{R}^+$ , where the  $\mathbb{R}^+ = [0, \infty)$  is scaling. The infinitesimal generator for scaling is identity  $L_2 = I$ . This group is also Abelian, meaning  $[L_2, L] = 0$  ( $L \in so(2)$  equation 38).  $\mathbb{R}^2/0$  can be lifted to  $G$  by choosing  $\mathbf{x}_0 = (1, 0)$  in polar coordinates and  $\mathbf{x} = g\mathbf{x}_0 = rL_2 \exp[\theta L]\mathbf{x}_0$ . We again have  $gL \cdot df/dg = \partial_\theta f$ . We also have  $gL_2 = g$ , so  $gL_2\mathbf{x}_0 = (x, y)$  and from equation 36,  $gL_2 \cdot df/dg = (x\partial_x + y\partial_y)f = r\partial_r f$ , which is the scaling operation.

### A.2.1 Rotation $SO(2)$

With  $\mathbf{x}_0 = (r, 0)$

$$g = \begin{pmatrix} \cos \theta & -\sin \theta \\ \sin \theta & \cos \theta \end{pmatrix}, = \frac{1}{r} \begin{pmatrix} x & -y \\ y & x \end{pmatrix}, \quad L = \begin{pmatrix} 0 & -1 \\ 1 & 0 \end{pmatrix} \quad gL = \frac{1}{r} \begin{pmatrix} -y & -x \\ x & -y \end{pmatrix} \quad (39)$$

$$gL\mathbf{x}_0 = \begin{pmatrix} -y \\ x \end{pmatrix} = \begin{pmatrix} -\sin \theta \\ \cos \theta \end{pmatrix} \quad (40)$$

To calculate  $df/dg$  we note that even after the lift, the function  $f$  was defined on  $\mathcal{S}$ . So we must include the  $\mathbf{x}_0$  in  $f(g\mathbf{x}_0)$ . Using equation 8, we have

$$\begin{aligned} \frac{df(g\mathbf{x}_0)}{dg} &= \frac{1}{r} \mathbf{x}_0^T \begin{pmatrix} \partial_x f & -\partial_y f \\ \partial_y f & \partial_x f \end{pmatrix} = \begin{pmatrix} \partial_x f & -\partial_y f \\ 0 & 0 \end{pmatrix} \\ gL \cdot \frac{df}{dg} &= \text{Tr} \begin{pmatrix} x\partial_y f - y\partial_x f & x\partial_x f + y\partial_y f \\ 0 & 0 \end{pmatrix} = (x\partial_y f - y\partial_x f) \end{aligned} \quad (41)$$

### A.2.2 Translations $T_n$

Generalizing the  $T_1$  case, we add a dummy dimension 0 and  $\mathbf{x}_0 = (1, 0, \dots, 0)$ . The generators are  $[\hat{L}_i]^\nu_\mu = \delta_{i\mu}\delta_0^\nu$  and  $g = I + x^i L_i$ . Again,  $gL_i = L_i + x^j L_j L_i = L_i$  as  $L_j L_i = 0$  for all  $i, j$ . Hence,  $[\hat{L}_i]^\alpha = [gL_i \mathbf{x}_0]^\alpha = \delta_i^\alpha$ .

### A.3 Group invariant loss

Because  $G$  is the symmetry group,  $f$  and  $g \cdot f$  should result in the same optimal parameters. Hence, the minima of the loss function need to be *group invariant*. One way to satisfy this is for the loss itself to be group invariant, which can be constructed by integrating over  $G$  (global pooling (Bronstein et al., 2021)). A function  $I = \int_G dg F(g)$  is  $G$ -invariant as for  $w \in G$

$$w \cdot I = \int_G w \cdot F(g) dg = \int F(w^{-1}g) dg = \int_G F(g') d(wg') = \int_G F(g') dg' \quad (42)$$

where we used the invariance of the Haar measure  $d(wg') = dg'$ . We can change the integration to  $\int_{\mathcal{S}} d^n x$  by change of variable  $dg/dx$ . Since we need  $\mathcal{S}$  to be lifted to  $G$ , the lift:  $\mathcal{S} \rightarrow G$  is injective, the a map  $G \rightarrow \mathcal{S}$  need not be.  $\mathcal{S}$  is homeomorphic to  $G/H$ , where  $H \subset G$  is the stabilizer of the origin, i.e.  $h\mathbf{x}_0 = \mathbf{x}_0, \forall h \in H$ . Since  $F(g\mathbf{x}_0) = F(gh\mathbf{x}_0)$ , we have

$$I = \int_G F(g) dg = \int_H dh \int_{G/H} dg' F(g') = V_H \int_{G/H} dg' F(g') \quad (43)$$

Since  $G/H \sim \mathcal{S}$ , the volume forms  $dg' = V_H d^n x$  can be matched for some parametrization.

#### A.3.1 MSE Loss

The MSE is given by  $I = \sum_n \int_G dg \|Q[f_n](g)\|^2$ , where  $f_n$  are data samples and  $Q[f]$  is L-conv or another  $G$ -equivariant function. In supervised learning the input is a pair  $f_n, y_n$ .  $G$  can also act on the labels  $y_n$ . We assume that  $y_n$  are either also scalar features  $y_n : \mathcal{S} \rightarrow \mathbb{R}^{m_y}$  with a group action  $g \cdot y_n(\mathbf{x}) = y_n(g^{-1}\mathbf{x})$  (e.g.  $f_n$  and  $y_n$  are both images), or that  $y_n$  are categorical. In the latter case  $g \cdot y_n = y_n$  because the only representations of a continuous  $G$  on a discrete set are constant. We can concatenate the inputs to  $\phi_n \equiv [f_n | y_n]$  with a well-defined  $G$  action  $g \cdot \phi_n = [g \cdot f_n | g \cdot y_n]$ . The collection of combined inputs  $\Phi = (\phi_1, \dots, \phi_N)^T$  is an  $(m + m_y) \times N$  matrix. Using equations 6 and 8, the MSE loss with parameters  $W = \{W^0, \bar{\epsilon}\}$  becomes

$$\begin{aligned} I[\Phi; W] &= \int_G dg \mathcal{L}[\Phi; W] = \int_G dg \left\| W^0 \left[ I + \bar{\epsilon}^i [\hat{L}_i]^\alpha \partial_\alpha \right] \Phi(g) \right\|^2 \\ &= 2 \int_G dg \left[ \|W^0 \Phi\|^2 + \|W^i [\hat{L}_i]^\alpha \partial_\alpha \Phi\|^2 + 2\Phi^T W^{0T} W^i [\hat{L}_i]^\alpha \partial_\alpha \Phi \right] \end{aligned} \quad (44)$$

$$= \int_{\mathcal{S}} \frac{d^n x}{\left| \frac{\partial x}{\partial g} \right|} \left[ \Phi^T \mathbf{m}_2 \Phi + \partial_\alpha \Phi^T \mathbf{h}^{\alpha\beta} \partial_\beta \Phi + [\hat{L}_i]^\alpha \partial_\alpha (\Phi^T \mathbf{v}^i \Phi) \right] \quad (45)$$

where  $\left| \frac{\partial x}{\partial g} \right|$  is the determinant of the Jacobian,  $W^i = W^0 \bar{\epsilon}^i$  and

$$\mathbf{m}_2 = W^{0T} W^0, \quad \mathbf{h}^{\alpha\beta}(\mathbf{x}) = \bar{\epsilon}^{iT} \mathbf{m}_2 \bar{\epsilon}^j [\hat{L}_i]^\alpha [\hat{L}_j]^\beta, \quad \mathbf{v}^i = \mathbf{m}_2 \bar{\epsilon}^i. \quad (46)$$

From equation 44 to 45 we used the fact that  $W^0$  and  $W^i$  do not depend on  $\mathbf{x}$  (or  $g$ ) to write

$$2\Phi^T W^{0T} W^i [\hat{L}_i]^\alpha \partial_\alpha \Phi = [\hat{L}_i]^\alpha \partial_\alpha (\Phi^T W^{0T} W^i \Phi) = [\hat{L}_i]^\alpha \partial_\alpha (\Phi^T \mathbf{m}_2 \bar{\epsilon}^i \Phi) \quad (47)$$

Note that  $\mathbf{h}$  has feature space indices via  $[\bar{\epsilon}^{iT} \mathbf{m}_2 \bar{\epsilon}^j]_{ab}$ , with index symmetry  $\mathbf{h}_{ab}^{\alpha\beta} = \mathbf{h}_{ba}^{\beta\alpha}$ . When  $\mathcal{F} = \mathbb{R}$  (i.e.  $f$  is a 1D scalar),  $\mathbf{h}^{\alpha\beta}$  becomes a Riemannian metric for  $\mathcal{S}$ . In general  $\mathbf{h}$  combines a 2-tensor  $\mathbf{h}_{ab} = \mathbf{h}_{ab}^{\alpha\beta} \partial_\alpha \partial_\beta \in TS \otimes TS$  with an inner product  $h^T \mathbf{h}^{\alpha\beta} f$  on the feature space  $\mathcal{F}$ . Hence  $\mathbf{h} \in TS \otimes TS \otimes \mathcal{F}^* \otimes \mathcal{F}^*$  is a (2, 2)-tensor, with  $\mathcal{F}^*$  being the dual space of  $\mathcal{F}$ .

**Loss invariant metric transformation** The metric  $\mathbf{h}$  transforms equivariantly as a 2-tensor. As discussed under equation 8,  $[\hat{L}_i(v\mathbf{x})]^\alpha = v_\beta^\alpha \hat{L}_i(\mathbf{x})^\beta$  and

$$v \cdot \mathbf{h}^{\alpha\beta} = \mathbf{h}^{\alpha\beta}(v^{-1}\mathbf{x}) = [v^{-1}]_\rho^\alpha [v^{-1}]_\gamma^\beta \mathbf{h}^{\rho\gamma}(\mathbf{x}), \quad (v \in G). \quad (48)$$

Note that  $v \cdot \mathbf{m}_2 = \mathbf{m}_2$  since  $f_n$  and  $y_n$  are scalars. For example, let  $G = SO(2)$  and  $R(\xi) \in SO(2)$  be rotation by angle  $\xi$ . Since there is only one  $L_i = L$ , the metric factorizes to

$$\mathbf{h}_{ab}^{\alpha\beta} = [\bar{\epsilon}^T \mathbf{m}_2 \bar{\epsilon}]_{ab} \otimes [\hat{L} \hat{L}^T]^{\alpha\beta} \quad (49)$$

To find  $R(\xi) \cdot \mathbf{h}$  we only need to calculate  $R(\xi)^{-1} \hat{L}$ . With  $g = R(\theta)$ , we have  $\hat{L}(\mathbf{x}) = R(\theta) L \mathbf{x}_0 = (-y, x) = r(-\sin \theta, \cos \theta)$  from equation 40. Therefore,  $R(\xi)^{-1} \hat{L} = R(\theta - \xi) = \hat{L}(R(\xi^{-1})\mathbf{x})$ . Using equation 21 in equation 48, the transformed metric becomes

$$R(\xi) \cdot \mathbf{h}^{\alpha\beta}(R(\theta)\mathbf{x}_0) = \bar{\epsilon}^T \mathbf{m}_2 \bar{\epsilon} \otimes [R(-\xi) \hat{L}]^\alpha [R(-\xi) \hat{L}]^\beta = \mathbf{h}^{\alpha\beta}(R(\theta - \xi)\mathbf{x}_0), \quad (50)$$

### A.3.2 Third term as a boundary term

Since terms in equation 20 are scalars, they can be evaluated in any basis. If  $\mathcal{S}$  can be lifted to multiple Lie groups, either group can be used to evaluate equation 20. For example  $\mathbb{R}^n/0$  can be lifted to both  $T_n$  and  $SO(n) \times \mathbb{R}_+$ . For the translation group  $G = T_n$  we have  $gL_i = L_i$  and  $[\hat{L}_i]^\alpha = \delta_i^\alpha$  (SI A.2.2) and  $|\partial g / \partial x| = 1$  and  $dg = d^n x$ . Thus, the last term in equation 20 simplifies to a complete divergence  $\int d^n x \partial_i (\Phi^T \mathbf{v}^i \Phi)$ . Using the generalized Stoke's theorem  $\int_{\mathcal{S}} dw = \int_{\partial \mathcal{S}} w$ , the last term in equation 20 becomes a boundary term. When  $\mathcal{S}$  is non-compact, the last term is  $I_\partial = \int_{\partial \mathcal{S}} d\Sigma_i \Phi^T \mathbf{v}^i \Phi$ , where  $d\Sigma_i$  is the normal times the volume form of the  $(n-1)$ D boundary  $\partial \mathcal{S}$  and is in the radial direction (e.g. for  $\mathcal{S} = \mathbb{R}^n$  the boundary is a hyper-sphere  $\partial \mathcal{S} = S^{n-1}$ ). Generally we expect the features  $\phi_n$  to be concentrated in a finite region of the space and that they go to zero as  $r \rightarrow \infty$  (if they don't the loss term  $\Phi^T \mathbf{m}_2 \Phi$  will diverge). Thus, the last term in equation 20 generally becomes a vanishing boundary term and does not matter.

### A.3.3 MSE Loss for translation group $T_n$

We have  $gL_i = L_i$  and  $[\hat{L}_i]^\alpha = \delta_i^\alpha$  (SI A.2.2), the last term in equation 20 becomes a complete divergence  $I_\partial = \int d^n x \partial_i (\Phi^T \mathbf{v}^i \Phi)$ . Using the generalized Stoke's theorem  $\int_{\mathcal{S}} dw = \int_{\partial \mathcal{S}} w$ , when  $\mathcal{S}$  is non-compact,  $I_\partial = \int_{\partial \mathcal{S}} d\Sigma_i \Phi^T \mathbf{v}^i \Phi$ . Here  $d\Sigma_i$  is the normal times the volume form of the  $(n-1)$ D boundary  $\partial \mathcal{S}$  (e.g. for  $\mathcal{S} = \mathbb{R}^n$  the boundary is a hyper-sphere  $\partial \mathcal{S} = S^{n-1}$ ). Generally we expect the features  $\phi_n$  to be concentrated in a finite region of the space and that they go to zero as  $r \rightarrow \infty$  (if they don't the loss term  $\Phi^T \mathbf{m}_2 \Phi$  will diverge). Thus, the last term in equation 20 generally becomes a vanishing boundary term and does not matter.

Next, the second term in equation 20 can be worked out as

$$\hat{L}_i^\alpha \partial_\alpha \phi^T \bar{\epsilon}^{iT} \mathbf{m}_2 \bar{\epsilon}^j \hat{L}_j^\beta \partial_\beta \phi = \partial_j \phi^T \bar{\epsilon}^{iT} \mathbf{m}_2 \bar{\epsilon}^j \partial_i \phi = \partial_j \phi^T \mathbf{h}^{ji} \partial_i \phi \quad (51)$$

where  $\mathbf{h}^{ji} = \bar{\epsilon}^{iT} \mathbf{m}_2 \bar{\epsilon}^j$  is a general, space-independent metric compatible with translation symmetry. When the weights  $[W^i]_b^a \sim \mathcal{N}(0, 1)$  are random Gaussian, we have  $W^{jT} W^i \approx m^2 \delta^{ij}$  and we recover the Euclidean metric. With the 1st term vanishing, the loss function equation 20 has a striking resemblance to a Lagrangian used in physics, as we discuss next.

### A.3.4 Boundary term with spherical symmetry

When  $\mathcal{S} \sim \mathbb{R}^n$  and  $G = T_n$ , the third term becomes a boundary term. But we can also have  $G = SO(n) \times \mathbb{R}_+$  (spherical symmetry and scaling). The boundary  $\partial \mathcal{S} \sim S^{n-1}$ , which has an  $SO(n)$  symmetry. The normal  $d\Sigma(\mathbf{x})$  is a vector pointing in the radial direction and  $g$  is the lift for  $\mathbf{x}$ . Since  $g \in SO(n)$ , we have

$$d\Sigma_\beta [gL_\alpha \mathbf{x}_0]^\beta = d\Sigma^T g L_\alpha \mathbf{x}_0 = [g^T d\Sigma]^T L_\alpha \mathbf{x}_0 \quad (52)$$

Since  $g \in SO(n)$ ,  $g^T = g^{-1}$  and  $g^T d\Sigma(g\mathbf{x}_0) = d\Sigma(\mathbf{x}_0) = V_{n-1}\mathbf{x}_0$ , meaning the normal vector is rotated back toward  $\mathbf{x}_0$ . Here  $V_{n-1}$  is the volume of the boundary  $S^{n-1}$ . Hence we have

$$d\Sigma^T g L_i \mathbf{x}_0 = \mathbf{x}_0^T L_i \mathbf{x}_0 = 0 \quad (53)$$

for all generators  $L_i \in so(n)$  because  $L_i = -L_i^T$  and hence diagonal entries like  $\mathbf{x}_0^T L_i \mathbf{x}_0$  are zero. Only the scaling generator  $L_0 = I$  we have  $\mathbf{x}_0^T L_0 \mathbf{x}_0 = 1$ . This means that the last term in equation 20 can be nonzero at the boundary only if  $\Phi \mathbf{v}^i \Phi$  is in the radial direction, meaning  $\bar{\epsilon}^0 = 0$ , and  $\Phi$  does not vanish at the boundary. However, a non-vanishing  $\Phi$  at the boundary results in diverging loss unless the mass matrix  $\mathbf{m}_2$  has eigenvalues equal to zero. This is what happens relativistic theories where light rays can have nonzero  $\Phi$  at infinity because they are massless.

#### A.4 Generalization error

Equivariant neural networks are hoped to be more robust than others. Equivariance should improve generalization. One way to check this is to see how the network would perform for an input  $\phi' = \phi + \delta\phi$  which adds a small perturbation  $\delta\phi$  to a real data point  $\phi$ . Robustness to such perturbation would mean that, for optimal parameters  $W^*$ , the loss function would not change, i.e.  $I[\phi'; W^*] = I[\phi; W^*]$ . This can be cast as a variational equation, requiring  $I$  to be minimized around real data points  $\phi$ . Writing  $I[\phi; W] = \int d^n x \mathcal{L}[\phi; W]$ , we have

$$\delta I[\phi; W^*] = \int_S d^n x \left[ \frac{\partial \mathcal{L}}{\partial \phi^a} \delta \phi^a + \frac{\partial \mathcal{L}}{\partial (\partial_\alpha \phi^a)} \partial_\alpha (\delta \phi^a) \right] \quad (54)$$

Doing a partial integration on the second term, we get

$$\begin{aligned} \delta I[\phi; W^*] &= \int_S d^n x \left[ \frac{\partial \mathcal{L}}{\partial \phi^b} - \partial_\alpha \frac{\partial \mathcal{L}}{\partial (\partial_\alpha \phi^b)} \right] \delta \phi^b + \int_S d^n x \partial_\alpha \left[ \frac{\partial \mathcal{L}}{\partial (\partial_\alpha \phi^b)} \delta \phi^b \right] \\ &= \int_S d^n x \left[ \frac{\partial \mathcal{L}}{\partial \phi^b} - \partial_\alpha \frac{\partial \mathcal{L}}{\partial (\partial_\alpha \phi^b)} \right] \delta \phi^b + \int_{\partial S} d^{n-1} \Sigma_\alpha \left[ \frac{\partial \mathcal{L}}{\partial (\partial_\alpha \phi^b)} \delta \phi^b \right] \end{aligned} \quad (55)$$

where we used the Stoke's theorem again to change the last term to a boundary integral. We will discuss this term further below, but since features  $\phi$  have to finite in extent,  $\phi(\mathbf{x}) \rightarrow 0$  as  $|\mathbf{x}| \rightarrow \infty$ , and the boundary term vanishes. We will return to the boundary integral below. The first term in equation 55 is the classic Euler-Lagrange (EL) equation. Thus, requiring good generalization, i.e.  $\delta I[\phi; W^*]/\delta \phi = 0$  means for optimal parameters  $W^*$ , the real data  $\phi$  satisfies the EL equations

$$\text{Generalization Error Minimization} \iff \text{EL: } \frac{\partial \mathcal{L}}{\partial \phi^b} - \partial_\alpha \frac{\partial \mathcal{L}}{\partial (\partial_\alpha \phi^b)} = 0 \quad (56)$$

Applying this to the MSE loss equation 20, equation 56 becomes

$$\mathbf{m}_2 \phi - \partial_\alpha (|J| \mathbf{h}^{\alpha\beta} \partial_\beta \phi) - \partial_\alpha (|J| \mathbf{v}^i [L_i]^\alpha) \phi = 0 \quad (57)$$

where  $|J| = |\partial g / \partial x|$  is the determinant of the Jacobian. For the translation group, equation 57 becomes a Helmholtz equation

$$\mathbf{h}^{ij} \partial_i \partial_j \phi = \bar{\epsilon}^i \mathbf{m}_2 \bar{\epsilon}^j \partial_i \partial_j \phi = \mathbf{m}_2 \phi \quad (58)$$

where  $\mathbf{h}^{ij} \partial_i \partial_j = \nabla^2$  is the Laplace-Beltrami operator with  $\mathbf{h}$  as the metric.

**Conservation laws** The equivariance condition equation 2 can be written for the integrand of the loss  $\mathcal{L}[\phi, W]$ . Since  $G$  is the symmetry of the system, transforming an input  $\phi \rightarrow w \cdot \phi$  by  $w \in G$  the integrand changes equivariantly as  $\mathcal{L}[w \cdot \phi] = w \cdot \mathcal{L}[\phi]$ . Now, let  $w$  be an infinitesimal  $w \approx I + \eta^i L_i$ . The action  $w \cdot \phi$  can be written as a Taylor expansion, similar to the one in L-conv, yielding

$$\begin{aligned} w \cdot \phi(\mathbf{x}) &= \phi(w^{-1} \mathbf{x}) = \phi((I - \eta^i L_i) \mathbf{x}) = \phi(\mathbf{x}) - \eta^i [L_i \mathbf{x}]^\alpha \partial_\alpha \phi(\mathbf{x}) \\ &= \phi(\mathbf{x}) + \delta \mathbf{x}^\alpha \partial_\alpha \phi(\mathbf{x}) = \phi(\mathbf{x}) + \delta \phi(\mathbf{x}) \end{aligned} \quad (59)$$

with  $\delta \mathbf{x}^\alpha = -\eta^i [L_i \mathbf{x}]^\alpha$  and  $\delta \phi = \delta \mathbf{x}^\alpha \partial_\alpha \phi$ . Similarly, we have  $w \cdot \mathcal{L} = \mathcal{L} + \delta \mathbf{x}^\alpha \partial_\alpha \mathcal{L}$ . Next, we can use the chain rule to calculate  $\mathcal{L}[w \cdot \phi]$ .

$$\begin{aligned} \mathcal{L}[w \cdot \phi] &= \mathcal{L}[\phi(\mathbf{x}) + \delta \phi(\mathbf{x})] = \mathcal{L}[\phi] + \frac{\partial \mathcal{L}}{\partial \phi^b} \delta \phi^b + \frac{\partial \mathcal{L}}{\partial (\partial_\alpha \phi^b)} \delta \partial_\alpha \phi^b \\ &= \mathcal{L}[\phi] + \left[ \frac{\partial \mathcal{L}}{\partial \phi^b} - \partial_\alpha \frac{\partial \mathcal{L}}{\partial (\partial_\alpha \phi^b)} \right] \delta \phi^b + \partial_\alpha \left( \frac{\partial \mathcal{L}}{\partial (\partial_\alpha \phi^b)} \delta \phi^b \right) \end{aligned} \quad (60)$$

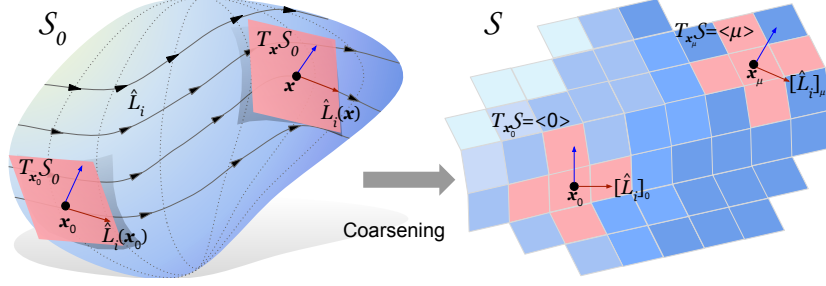


Figure 5: **Manifold vs. discretized Space** While real systems can have a continuous manifold  $\mathcal{S}_0$  as their base space, often the data collected from is a discrete array  $\mathcal{S}$ . The discretization (coarsening) will induce some of the topology of  $\mathcal{S}_0$  on  $\mathcal{S}$  as a graph. Graph neighborhoods  $\langle \mu \rangle$  on the discrete  $\mathcal{S}$  represent tangent spaces  $T_{\mathbf{x}_\mu} \mathcal{S}$  and approximate  $T_{\mathbf{x}} \mathcal{S}_0$ . The lift takes  $\mathbf{x} \in \mathcal{S}_0$  to  $g \in G$ , and maps the tangent spaces  $T_{\mathbf{x}} \mathcal{S}_0 \rightarrow T_g G$ . Each Lie algebra basis  $L_i \in \mathfrak{g} = T_1 G$  generates a vector field on the tangent bundle  $TG$  via the pushforward as  $L^{(g)} = gL_i g^{-1}$ . Due to the lift, each  $L_i$  also generates a vector field  $\hat{L}_i^\alpha(\mathbf{x}) \partial_\alpha = [gL_i \mathbf{x}_0]^\alpha \partial_\alpha$ , with  $\mathbf{x} = g\mathbf{x}_0$ . Analogously, on  $\mathcal{S}$  we get a vector field  $[\hat{L}_i]_\mu = g_\mu L_i \mathbf{x}_0$  on  $T\mathcal{S}$ , with  $\mathbf{x}_\mu = g_\mu \mathbf{x}_0$ . Note that depicting  $\mathcal{S}$  and  $\mathcal{S}_0$  as 2D is only for convenience. They may have any dimensions.

where we used the fact that  $\delta \mathbf{x} = \eta^i L_i \mathbf{x}$  can vary independently from  $\mathbf{x}$  (because of  $\eta^i$ ), and so  $\delta \partial_\alpha \phi^b = \partial_\alpha \delta \phi^b$ . The same way,  $\delta \mathbf{x}^\alpha \partial_\alpha \mathcal{L} = \partial_\alpha (\delta \mathbf{x}^\alpha \mathcal{L})$ . Now, if  $\phi$  are the real data and the parameters in  $\mathcal{L}$  minimize generalization error, then  $\mathcal{L}$  satisfies equation 57. This means that the first term in equation 60 vanishes. Setting the second term equal to  $w \cdot \mathcal{L}$  we get

$$\mathcal{L}[w \cdot \phi] - w \cdot \mathcal{L}[\phi] = \partial_\alpha \left[ \frac{\partial \mathcal{L}}{\partial (\partial_\alpha \phi^b)} \delta \phi^b - \delta \mathbf{x}^\alpha \mathcal{L} \right] = 0 \quad (61)$$

Thus, the terms in the brackets are divergence free. These terms are called a Noether conserved current  $J^\alpha$ . In summary

$$\text{Noether current: } J^\alpha = \frac{\partial \mathcal{L}}{\partial (\partial_\alpha \phi^b)} \delta \phi^b - \frac{\partial \mathcal{L}}{\partial \mathbf{x}^\alpha} \delta \mathbf{x}^\alpha, \quad \delta I[\phi; W^*] = 0 \Rightarrow \partial_\alpha J^\alpha = 0 \quad (62)$$

$J$  captures the change of the Lagrangian  $\mathcal{L}$  along symmetry direction  $\hat{L}_i$ . Plugging  $\delta \phi = \delta \mathbf{x}^\alpha \partial_\alpha \phi$  from equation 59 we find

$$\partial_\alpha \left[ \frac{\partial \mathcal{L}}{\partial (\partial_\alpha \phi^b)} \delta \phi^b - \delta \mathbf{x}^\alpha \mathcal{L} \right] = \delta \mathbf{x}^\beta \partial_\alpha \left[ \frac{\partial \mathcal{L}}{\partial (\partial_\alpha \phi^b)} \partial_\beta \phi^b - \delta_\beta^\alpha \mathcal{L} \right] = \delta \mathbf{x}^\beta \partial_\alpha T_\beta^\alpha. \quad (63)$$

$T_\beta^\alpha$  is known as the stress-energy tensor in physics (Landau, 2013). It is the Noether current associated with space (or space-time) variations  $\delta \mathbf{x}$ . It appears here because  $G$  acts on the space, as opposed to acting on feature dimensions. For the MSE loss we have

$$T_\beta^\alpha \equiv \frac{\partial \mathcal{L}}{\partial (\partial_\alpha \phi^b)} \partial_\beta \phi^b - \delta_\beta^\alpha \mathcal{L} = \partial_\rho \phi^T (\delta_\beta^\lambda \mathbf{h}^{\alpha\rho} - \delta_\beta^\alpha \mathbf{h}^{\rho\lambda}) \partial_\lambda \phi - \phi^T \mathbf{m}_2 \phi \quad (64)$$

It would be interesting to see if the conserved currents can be used in practice as an alternative way for identifying or discovering symmetries.

## B Tensor notation details

If the dataset being analyzed is in the form of  $f(\mathbf{x})$  for some sample of points  $\mathbf{x}$ , together with derivatives  $\nabla f(\mathbf{x})$ , we can use the L-conv formulation above. However, in many datasets, such as images,  $f(\mathbf{x})$  is given as a finite dimensional array or tensor, with  $\mathbf{x}$  taking values over a grid. Even though the space  $\mathcal{S}$  is now discrete, the group which acts on it can still be continuous (e.g. image rotations). Let  $\mathcal{S} = \{\mathbf{x}_0, \dots, \mathbf{x}_{d-1}\}$  contain  $d$  points. Each  $\mathbf{x}_\mu$  represents a coordinate in higher dimensional grid. For instance, on a  $10 \times 10$  image,  $\mathbf{x}_0$  is  $(x, y) = (0, 0)$  point and  $\mathbf{x}_{99}$  is  $(x, y) = (9, 9)$ .

**Feature maps** To define features  $f(\mathbf{x}_\mu) \in \mathbb{R}^m$  for  $\mathbf{x}_\mu \in \mathcal{S}$ , we embed  $\mathbf{x}_\mu \in \mathbb{R}^d$  and encode them as the canonical basis (one-hot) vectors with components  $[\mathbf{x}_\mu]^\nu = \delta_\mu^\nu$  (Kronecker delta), e.g.  $\mathbf{x}_0 = (1, 0, \dots, 0)$ . The feature space becomes  $\mathcal{F} = \mathbb{R}^d \otimes \mathbb{R}^m$ , meaning feature maps  $\mathbf{f} \in \mathcal{F}$  are  $d \times m$  tensors, with  $f(\mathbf{x}_\mu) = \mathbf{x}_\mu^T \mathbf{f} = \mathbf{f}_\mu$ .

**Group action** Any subgroup  $G \subseteq \text{GL}_d(\mathbb{R})$  of the general linear group (invertible  $d \times d$  matrices) acts on  $\mathbb{R}^d$  and  $\mathcal{F}$ . Since  $\mathbf{x}_\mu \in \mathbb{R}^d$ ,  $g \in G$  also naturally act on  $\mathbf{x}_\mu$ . The resulting  $\mathbf{y} = g\mathbf{x}_\mu$  is a linear combination  $\mathbf{y} = c^\nu \mathbf{x}_\nu$  of elements of the discrete  $\mathcal{S}$ , not a single element. The action of  $G$  on  $\mathbf{f}$  and  $\mathbf{x}$ , can be defined in multiple equivalent ways. We define  $f(g \cdot \mathbf{x}_\mu) = \mathbf{x}_\mu^T g^T \mathbf{f}$ ,  $\forall g \in G$ . For  $w \in G$  we have

$$w \cdot f(\mathbf{x}_\mu) = f(w^{-1} \cdot \mathbf{x}_\mu) = \mathbf{x}_\mu^T w^{-1T} \mathbf{f} = [w^{-1} \mathbf{x}]^T \mathbf{f} \quad (65)$$

Dropping the position  $\mathbf{x}_\mu$ , the transformed features are matrix product  $w \cdot \mathbf{f} = w^{-1T} \mathbf{f}$ .

**G-conv and L-conv in tensor notation** Writing G-conv equation 3 in the tensor notation we have

$$[\kappa \star \mathbf{f}](g\mathbf{x}_0) = \int_G \kappa(v) f(gv\mathbf{x}_0) dv = \mathbf{x}_0^T \int_G v^T g^T \mathbf{f} \kappa^T(v) dv \equiv \mathbf{x}_0^T [\mathbf{f} \star \kappa](g) \quad (66)$$

where we moved  $\kappa^T(v) \in \mathbb{R}^m \otimes \mathbb{R}^{m'}$  to the right of  $\mathbf{f}$  because it acts as a matrix on the output index of  $\mathbf{f}$ . The equivariance of equation 66 is readily checked with  $w \in G$

$$w \cdot [\mathbf{f} \star \kappa](g) = [\mathbf{f} \star \kappa](w^{-1}g) = \int_G v^T g^T w^{-1T} \mathbf{f} \kappa^T(v) dv = [(w \cdot \mathbf{f}) \star \kappa](g) \quad (67)$$

where we used  $[w^{-1}g]^T \mathbf{f} = g^T w^{-1T} \mathbf{f}$ . Similarly, we can rewrite L-conv equation 6 in the tensor notation. Defining  $v_\epsilon = I + \bar{\epsilon}^i L_i$

$$\begin{aligned} Q[\mathbf{f}](g) &= W^0 f(g(I + \bar{\epsilon}^i L_i)) = \mathbf{x}_0^T (I + \bar{\epsilon}^i L_i)^T g^T \mathbf{f} W^{0T} \\ &= (\mathbf{x}_0 + \bar{\epsilon}^i [g L_i \mathbf{x}_0])^T \mathbf{f} W^{0T}. \end{aligned} \quad (68)$$

Here,  $\hat{L}_i = g L_i \mathbf{x}_0$  is exactly the tensor analogue of pushforward vector field  $\hat{L}_i$  in equation 8. We will make this analogy more precise below. The equivariance of L-conv in tensor notation is again evident from the  $g^T \mathbf{f}$ , resulting in

$$Q[w \cdot \mathbf{f}](g) = \mathbf{x}_0^T v_\epsilon^T g^T w^{-1T} \mathbf{f} W^{0T} = Q[\mathbf{f}](w^{-1}g) = w \cdot Q[\mathbf{f}](g) \quad (69)$$

Next, we will discuss how to implement equation 68 in practice and how to learn symmetries with L-conv. We will also discuss the relation between L-conv and other neural architectures.

## B.1 Constraints from topology on tensor L-conv

To implement equation 68 we need to specify the lift and the form of  $L_i$ . We will now discuss the mathematical details leading to an easy to implement form of equation 68.

**Topology** Although the discrete space  $\mathcal{S}$  is a set of points, in many cases it has a topology. For instance,  $\mathcal{S}$  can be a discretization of a manifold  $\mathcal{S}_0$ , or vertices on a lattice or a general graph. We encode this topology in an undirected graph (i.e. 1-simplex) with vertex set  $\mathcal{S}$  edge set  $\mathcal{E}$ . Instead of the commonly used graph adjacency matrix  $\mathbf{A}$ , we will use the incidence matrix  $\mathbf{B} : \mathcal{S} \times \mathcal{E} \rightarrow \{0, 1, -1\}$ .  $\mathbf{B}_\alpha^\mu = 1$  or  $-1$  if edge  $\alpha$  starts or ends at node  $\mu$ , respectively, and  $\mathbf{B}_\alpha^\mu = 0$  otherwise (undirected graphs have pairs of incoming and outgoing edges). Similar to the continuous case we will denote the topological space  $(\mathcal{S}, \mathcal{E}, \mathbf{B})$  simply by  $\mathcal{S}$ .

Figure 5 summarizes some of the aspects of the discretization as well as analogies between  $\mathcal{S}_0$  and  $\mathcal{S}$ . Technically, the group  $G_0$  acting on  $\mathcal{S}_0$  and  $G$  acting on  $\mathcal{S}$  are different. But we can find a group  $G$  which closely approximates  $G_0$  (see SI B.2). For instance, Rao & Ruderman (1999) used Shannon-Whittaker interpolation theorem (Whittaker, 1915) to define continuous 1D translation and 2D rotation groups on discrete data. We return to this when expressing CNN as L-conv in 5.

**Neighborhoods as discrete tangent bundle**  $\mathcal{B}$  is useful for extending differential geometry to graphs (Schaub et al., 2020). Define the neighborhood  $\langle \mu \rangle = \{\alpha \in \mathcal{E} \mid \mathbf{B}_\alpha^\mu = -1\}$  of  $\mathbf{x}_\mu$  as the set of outgoing edges.  $\langle \mu \rangle$  can be identified with  $T_{\mathbf{x}_\mu} \mathcal{S}$  as for  $\alpha \in \langle \mu \rangle$ ,  $\mathbf{B}_\alpha \mathbf{f} = \mathbf{f}_\mu - \mathbf{f}_\nu \sim \partial_\alpha \mathbf{f}$ , where  $\mu$  and  $\nu$  are the endpoints of edge  $\alpha$ . This relation becomes exact when  $\mathcal{S}$  is an  $n$ D square lattice with infinitesimal lattice spacing. The set of all neighborhoods is  $\mathcal{B}$  itself and encodes the approximate tangent bundle  $T\mathcal{S}$ . For some operator  $C : \mathcal{S} \otimes \mathcal{F} \rightarrow \mathcal{F}$  acting on  $\mathbf{f}$  we will say  $C \in \langle \mu \rangle$  if its action remains within vertices connected to  $\mu$ , meaning

$$C \in \langle \mu \rangle: \quad C\mathbf{f} = \sum_{\alpha \in \langle \mu \rangle} \tilde{C}^\alpha \mathbf{B}_\alpha^\nu \mathbf{f}_\nu \quad (70)$$

**Lift and group action** Lie algebra elements  $L_i$  by definition take the origin  $\mathbf{x}_0$  to points close to it. Thus, for small enough  $\eta$ ,  $(I + \eta L_i)\mathbf{x}_0 \in \langle 0 \rangle$  and so  $[L_i \mathbf{x}_0]^T \mathbf{f} = [\hat{L}_i]_0^\rho \mathbf{f}_\rho = \sum_{\alpha \in \langle 0 \rangle} [\hat{\ell}_i]_0^\alpha \mathbf{B}_\alpha^\rho \mathbf{f}_\rho$ . The coefficients  $[\hat{\ell}_i]_0^\alpha \in \mathbb{R}$  are in fact the discrete version of  $\hat{L}_i$  components from equation 8. For the pushforward  $g L_i g^{-1}$ , we define the lift via  $\mathbf{x}_\mu = g_\mu \mathbf{x}_0$ . We require the  $G$ -action to preserve the topology of  $\mathcal{S}$ , meaning points which are close remain close after the  $G$ -action. As a result,  $\langle \mu \rangle$  can be reached by pushing forward elements in  $\langle 0 \rangle$ . Thus, for each  $i$ ,  $\exists \eta \ll 1$  such that  $g_\mu (I + \eta L_i) \mathbf{x}_0 \in \langle \mu \rangle$ , meaning for a set of coefficients  $[\hat{L}_i]_\mu^\nu \in \mathbb{R}$  we have

$$[g_\mu (I + \eta L_i) \mathbf{x}_0]^T \mathbf{f} = \mathbf{f}_\mu + \eta \sum_{\alpha \in \langle \mu \rangle} [\hat{\ell}_i]_\mu^\alpha \mathbf{B}_\alpha^\nu \mathbf{f}_\nu \quad (71)$$

where  $\mathbf{f}_\mu = \mathbf{x}_\mu^T \mathbf{f}$ . Acting with  $[g_\mu L_i \mathbf{x}_0]^T \mathbf{x}_\nu$  and inserting  $I = \sum_\rho \mathbf{x}_\rho \mathbf{x}_\rho^T$  we have

$$\begin{aligned} [\hat{L}_i]_\mu^\nu &= [\hat{\ell}_i]_\mu^\alpha \mathbf{B}_\alpha^\nu = [g_\mu L_i \mathbf{x}_0]^\nu = \sum_\rho [g_\mu \mathbf{x}_\rho \mathbf{x}_\rho^T L_i \mathbf{x}_0]^T \mathbf{x}_\nu \\ &= \sum_{\rho \in \langle 0 \rangle} [L_i]_0^\rho [\mathbf{x}_\nu^T g_\mu \mathbf{x}_\rho]^T = [L_i]_0^\rho [g_\mu]_\rho^\nu = [\hat{\ell}_i]_0^\alpha \mathbf{B}_\alpha^\rho [g_\mu]_\rho^\nu \end{aligned} \quad (72)$$

This  $\hat{L}_i \equiv \hat{\ell}_i^\alpha \mathbf{B}_\alpha$  is the discrete  $\mathcal{S}$  version of the vector field  $\hat{L}_i(\mathbf{x}) = [g L_i \mathbf{x}_0]^\alpha \partial_\alpha$  in equation 8.

## B.2 Approximating a symmetry and discretization error

**Discretization error** While systems such as crystalline solids are discrete in nature, many other datasets such as images result from discretization of continuous data. The discretization (or ‘‘coarsening’’ (Bronstein et al., 2021)) will modify the groups that can act on the space. For example, first rotating a shape by  $SO(2)$  then taking a picture is different from first taking a picture then rotating the picture (i.e. group action and discretization do not commute). Nevertheless, in most cases in physics and machine learning the symmetry group  $G_0$  of the space before discretization has a small Lie algebra dimension  $n$ , (e.g.  $SO(3)$ ,  $SE(3)$ ,  $SO(3, 1)$  etc). Usually the resolution of the discretization is  $d \gg n$ . In this case, there always exist some  $G \subseteq GL_d(\mathbb{R})$  which approximates  $G_0$  reasonably well. The approximation means  $\forall g_0 \in G_0, \exists g \in G$  such that the error  $\mathcal{L}_G = \|g_0 \cdot f(\mathbf{x}_\mu) - \mathbf{x}_\mu^T g \mathbf{f}\|^2 < \eta^2$  where  $\eta$  depends on the resolution of the discretization. Minimizing the error  $\mathcal{L}_G$  can be the process of identifying the  $G$  which best approximates  $G_0$ . We will denote this approximate similarity as  $G \simeq G_0$ . For example, Rao & Ruderman (1999) used the Shannon-Whittaker Interpolation theorem (Whittaker, 1915) to translate discrete 1D signals (features) by arbitrary, continuous amounts. In this case the transformed features are  $\mathbf{f}'_\mu = g(z)_\mu^\nu \mathbf{f}_\nu$ , where  $g(z)_\mu^\nu = \frac{1}{d} \sum_{p=-d/2}^{d/2} \cos\left(\frac{2\pi p}{d}(z + \mu - \nu)\right)$  approximates the shift operator for continuous  $z$ . The  $g(z)$  form a group because  $g(w)g(z) = g(w + z)$ , which is a representation for periodic 1D shifts. Rao & Ruderman (1999) also use a 2D version of the interpolation theorem to approximate  $SO(2)$ . In practice, we can assume the true symmetry to be  $G$ , as we only have access to the discretized data and can’t measure  $G_0$  directly.

## C Experiments

We conduct a set of experiments to see how well L-conv can extract infinitesimal generators.

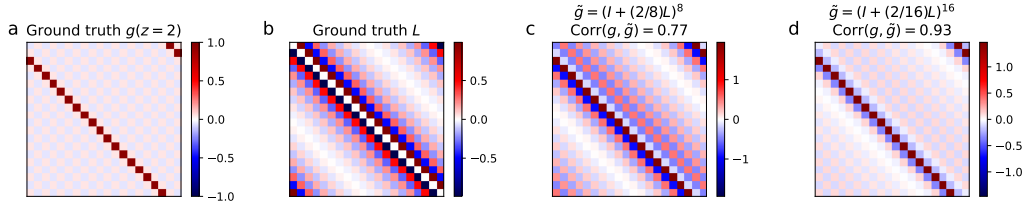


Figure 6: 1D Translation: Using the Shannon-Whittaker Interpolation (SWI) one can generate continuous shifts on discrete data. These include integer shifts (a, ground truth). (SWI) also yields an infinitesimal generator  $L$  for shifts (b). This  $L$  can be used to approximate finite shifts using  $\hat{g}_n(z) = (I + z/nL)^n$ , with  $n \rightarrow \infty$  yielding  $\exp[zL]$ . (c) and (d) show the approximation of a shift by two pixels using  $n = 8$  and  $n = 16$ .

**Nonlinear activation** As noted in Weiler et al. (2018a), an arbitrary nonlinear activation  $\sigma$  may not keep the architecture equivariant under  $G$ . However, as we showed in SI A (**Extended equivariance for L-conv**), the feature dimensions can pass through any nonlinear neural network without affecting the equivariance of L-conv. This means that the weights of the nonlinear layer should act only on  $\mathcal{F}$  and not  $\mathcal{S}$ .

**Implementation** The basic way to implement L-conv is as multiple parallel GCN units with aggregation function  $f(A)$  being (propagation rule) being  $\hat{L}_i$ . We do not use Deep Graph Library (DGL) or other libraries, as we want to make  $\hat{L}_i$  learnable for discovering symmetries. A more detailed way to implement L-conv is to encode  $\hat{L}_i$  in the form of equation 18 (equation 72) to ensure that there is an underlying shared generator  $\hat{\ell}_i$  for all  $\mu$  which is pushed forward using  $g_\mu$ , shared for all  $i$ . To implement L-conv this way, we need the lift  $g_\mu$  and the edge weights  $w_i^\alpha = [\hat{\ell}_i]_0^\alpha$ . With known symmetries, the learnable parameters are  $W^0$  and  $\bar{\epsilon}^i$ . When the topology and hence  $B$  is known, we can encode it into the geometry and only learn the edge weights  $[\hat{\ell}_i]_\mu^\alpha$ , similar to edge features in message passing neural networks (MPNN) (Gilmer et al., 2017). In general each  $\hat{\ell}_i$  has  $|\mathcal{E}|$  (i.e. number of edges) components. We can further reduce these using equation 18, where instead of  $n$  matrices  $\hat{\ell}_i$ , we learn one  $g_\mu$  shared for all, and a small set of elements  $[\hat{\ell}_i]_0^\alpha$ . This is easiest when the graph is a regular lattice and each vertex has the same number of neighbors. When the topology of the underlying space is not known (e.g. point cloud or scrambled coordinates), we can learn  $\hat{L}_i$  as  $d \times d$  matrices. We do this for the scrambled image tests, where we encode  $\hat{L}_i$  as low-rank matrices.

**Symmetry Discovery Literature** In addition to simplifying the construction of equivariant architectures, our method can also learn the symmetry generators from data. Learning symmetries from data has been studied before, but mostly in restricted settings. Examples include commutative Lie groups as in Cohen & Welling (2014), 2D rotations and translations in Rao & Ruderman (1999), Sohl-Dickstein et al. (2010) or permutations (Anselmi et al., 2019). Zhou et al. (2020) uses meta-learning to automatically learn symmetries in the data. Yet their weight-sharing scheme and the encoding of the symmetry generators is very different from ours. (Benton et al., 2020) propose Augerino, a method to learn equivariance with neural networks, but restricted to a subgroup of the augmentation transformations. Their Lie algebra is fixed to affine transformations in 2D (translations, rotations, scaling and shearing). Our approach is more general. We learn the  $L_i$  directly without restricting to known symmetries. Additionally, we do not use the exponential map or matrix logarithm, hence, our method is easy to implement. Lastly, Augerino uses sampling to effectively cover the space of group transformations. Since we work with the Lie algebra rather than the group itself, we do not require sampling.

### C.1 Approximating 1D CNN

As discussed in the text, Rao & Ruderman (1999, sec. 4) used the Shannon-Whittaker Interpolation (SWI) (Whittaker, 1915) to define continuous translation on periodic 1D arrays as  $\mathbf{f}'_\rho = g(z)_\rho^\nu \mathbf{f}_\nu$ . Here  $g(z)_\rho^\nu = \frac{1}{d} \sum_{p=-d/2}^{d/2} \cos\left(\frac{2\pi p}{d}(z + \rho - \nu)\right)$  approximates the shift operator for continuous  $z$ .

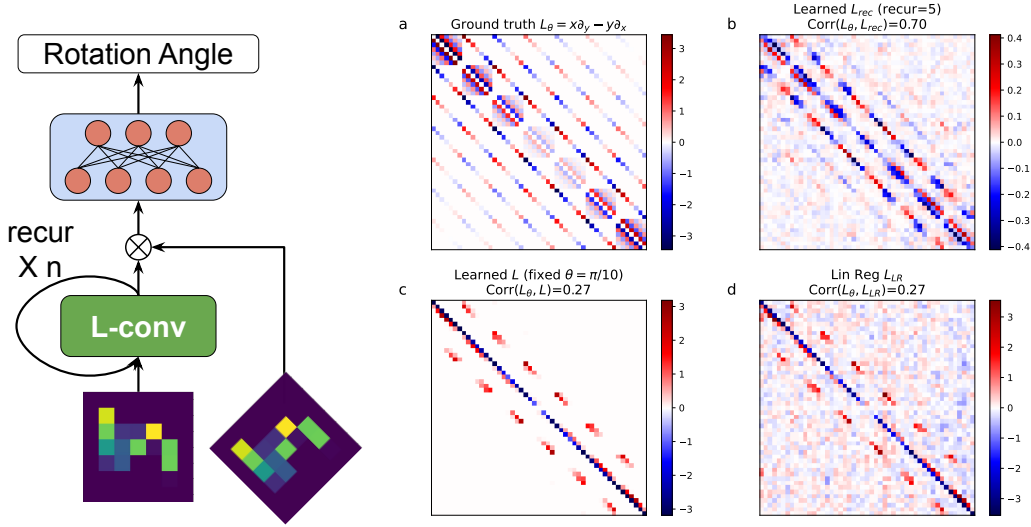


Figure 7: **Learning the infinitesimal generator of  $SO(2)$**  Left shows the architecture for learning rotation angles between pairs of images. (a) shows the rotation generator calculated analytically using Shannon-Whittaker interpolation. (b) is the  $\hat{L}$  learned using recursive L-conv learning rotation angle between a pair of images. (c) is an  $L$  learned using a fixed small rotation angle  $\theta = \pi/10$ , and (d) shows  $\hat{L}$  found using the numeric linear regression solution from the fixed angle data. (b) has the highest cosine correlation (0.70) with the ground truth, compared to 0.27 for  $\hat{L}$  extracted using small angles.

These  $g(z)$  form a 1D translation group  $G$  as  $g(w)g(z) = g(w+z)$  with  $g(0)_\rho^\nu = \delta_\rho^\nu$ . For any  $z = \mu \in \mathbb{Z}$ ,  $g_\mu = g(z = \mu)$  are circulant matrices that shift by  $\mu$  as  $[g_\mu]_\rho^\nu = \delta_{\nu-\mu}^\rho$ .  $g_\mu$  can be approximated using the Lie algebra and written as multi-layer L-conv as in sec. 3.2. Using  $g(0)_\rho^\nu \approx \delta(\rho - \nu)$ , the single Lie algebra basis  $[\hat{L}]_0 = \partial_z g(z)|_{z \rightarrow 0}$ , acts as  $\hat{L}f(z) \approx -\partial_z f(z)$  (because  $\int \partial_z \delta(z - \nu) f(z) = -\partial_\nu f(\nu)$ ). Its components are  $\hat{L}_\rho^\nu = L(\rho - \nu) = \sum_p \frac{2\pi p}{d^2} \sin\left(\frac{2\pi p}{d}(\rho - \nu)\right)$ , which are also circulant due to the  $(\rho - \nu)$  dependence. Hence,  $[\hat{L}\mathbf{f}]_\rho = \sum_\nu L(\rho - \nu)\mathbf{f}_\nu = [L \star \mathbf{f}]_\nu$  is a convolution. Rao & Ruderman (1999) already showed that this  $\hat{L}$  can reproduce finite discrete shifts  $g_\mu$  used in CNN. They used a primitive version of L-conv with  $g_\mu = (I + \epsilon \hat{L})^N$ . Thus, L-conv can approximate 1D CNN. This result generalizes easily to higher dimensions.

Figure 6 shows how this approximation works. (b) shows the analytical form of  $\hat{L}$ . (c) and (d) show two approximations of  $g_2 = g(z = 2)$ , shift by two pixels, using  $\tilde{g}(z) = (I + z/n\hat{L})^n$  with  $n = 8$  and  $n = 16$ . We can evaluate the quality of these approximations using their cosine correlation defined as  $\text{Corr}(g, \tilde{g}) = \text{Tr}[g^T \tilde{g}] / (\|g\| \|\tilde{g}\|)$  where  $\|A\| = \sqrt{\sum_{i,j} (A_j^i)^2}$  is the Frobenius  $L_2$  norm. (c) shows 0.77 correlation and (d) has 0.93.

## C.2 Extracting 2D rotation generator for fixed small rotations

**Ground truth** We can use the same SWI 1D translation generators discussed above for CNN as  $\partial_x$  and  $\partial_y$  to construct the rotation generator  $L_\theta = x\partial_y - y\partial_x$  (Fig. 7, a). We will use cosine correlation with this  $L_\theta$  to evaluate the quality of the learned  $\hat{L}$ . As we will find below, the best outcome is from  $\hat{L}$  learned using a recursive L-conv learning the angle of rotation between a pair of images (Fig. 7, b) with 0.70 correlation.

**Using fixed small angle** In the first experiment we try to learn a small rotation with angle  $\theta = \pi/10$  using a single layer L-conv (Fig. 7,c). This experiment was already done in (Rao & Ruderman, 1999). The input is a random  $7 \times 7$  image  $\mathbf{f}$  with pixels chosen in  $[-.5, 0.5)$ . The output  $\mathbf{f}'$  is the same image rotated by  $\theta$  using pytorch affine transform. Our training set contains 50,000 images., the test

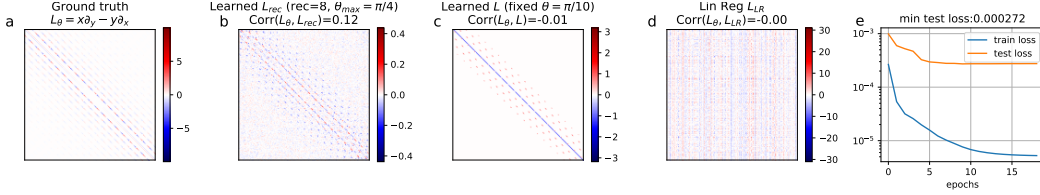


Figure 8: Learning  $\hat{L}$  via larger rotation angles for larger images. This time the correlation with ground truth  $L_\theta$  is much less, but accuracy is still very good.

set was 10,000 images, batch size was 64. The code was implemented in pytorch and we used the Adam optimizer with learning rate  $10^{-2}$ . The experiments were run for 20 epochs. This problem is simply a linear regression with  $\mathbf{f}' = R\mathbf{f} = (I + \epsilon\hat{L})\mathbf{f}$ . L-conv solves it using SGD and finds  $\epsilon\hat{L}$ . This problem can also be solved exactly using the solution to linear regression. Let  $X = (\mathbf{f}_1, \dots, \mathbf{f}_N)$  and  $Y = (\mathbf{f}'_1, \dots, \mathbf{f}'_N)$  be the matrix of all inputs and outputs, respectively. The rotation equation is  $Y^T = RX^T$ . Thus, the rotation matrix is given by  $R = (Y^T X)(X^T X)^{-1}$ . Figure 7 (c, d) shows the results of this experiment. The  $L$  found using L-conv with SGD is much cleaner than the numerical linear regression solution  $L_{LR} = (R - I)/\theta$ . The loss becomes extremely small both on training and test data.

### C.3 Learning rotation angle

In this experiment we have a pair of input images  $(\mathbf{f}_n, R(\theta_n)\mathbf{f}_n)$ , with  $R(\theta) \in SO(2)$  (approximating 2D rotations). The two inputs differ by a finite rotation with angle  $\theta_n \in [0, \pi/8)$ . The task is to learn the rotation angle  $\theta_n$ . For this task we use a recursive L-conv. We set  $W^0 = I$ . The L-conv weight  $\bar{\epsilon}$  is  $m \times m$ . To be able to encode multiple angles, we set  $m = 10$  and feed 10 copies of the  $\mathbf{f}_n$  as input  $\mathbf{h}_0 = [\mathbf{f}_n] \times 10$ . We pass this through the same L-conv layer  $t = 3$  times as  $\mathbf{h}_i = Q[\mathbf{h}_{i-1}]$ . In the final layer, we first take the dot product of the final output  $\mathbf{h}_t$  with the rotated input  $\mathbf{y}_n = R(\theta)\mathbf{f}_n$  to obtain  $\mathbf{g} = \tanh(\mathbf{y}_n^T \mathbf{h}_t)$ . We then pass the output  $\mathbf{g} \in \mathbb{R}^m$  through a fully-connected (FC) layer with 5 nodes and tanh activation, and finally through a linear FC layer with one output to obtain the angle. The batch size was 16, Adam optimizer, learning rate  $10^{-3}$ , rest were default.

Despite being a much harder task than fitting a fixed angle rotation, the learned  $\hat{L}$  of this experiment has the highest (0.70) cosine correlation with the ground truth  $L_\theta$  (Fig. 7, b). Even though the architecture is rather complicated and L-conv is followed by two MLP layers, the  $\hat{L}$  in L-conv learns the infinitesimal generator of rotations very well. We also conducted experiments with larger random images ( $20 \times 20$ ) and larger angles of rotation  $\theta_n \in [0, \pi/4)$  (Fig. 8). While the accuracy of learning the angles is still pretty good (Fig. 8, e, test loss  $2.7 \times 10^{-4}$ ) the larger angles result in less correlation between the learned  $\hat{L}$  and the ground truth  $L_\theta$  (Fig. 8, b, correlation 0.12 with 8 times recurrence). The learned  $\hat{L}$  is closer to a finite angle rotation. This may be because the with small number of recurrences the network found small but finite rotations approximate larger rotations better than using a true infinitesimal generator.

## D Experiments on Images

To understand precisely how L-conv performs in comparison with CNN and other baselines, we conduct a set of carefully designed experiments. Defining pooling for L-conv merits more research. Without pooling, we cannot use L-conv in state-of-the-art models for problems such as image classification. Therefore, we use the simplest possible models in our experiments: one or two L-conv, or CNN, or FC layers, followed by a classification layer. We do not use any other operations such as dropout or batch normalization in any of the experiments.

**Test Datasets** We use four datasets: MNIST, CIFAR10, CIFAR100, and FashionMNIST. To test the efficiency of L-conv in dealing with hidden or unfamiliar symmetries, we conducted our tests on two modified versions of each dataset: 1) **Rotated**: each image rotated by a random angle (no augmentation); 2) **Rotated and Scrambled**: random rotations are followed by a fixed random permutation (same for all images) of pixels. We used a 80-20 training test split on 60,000 MNIST

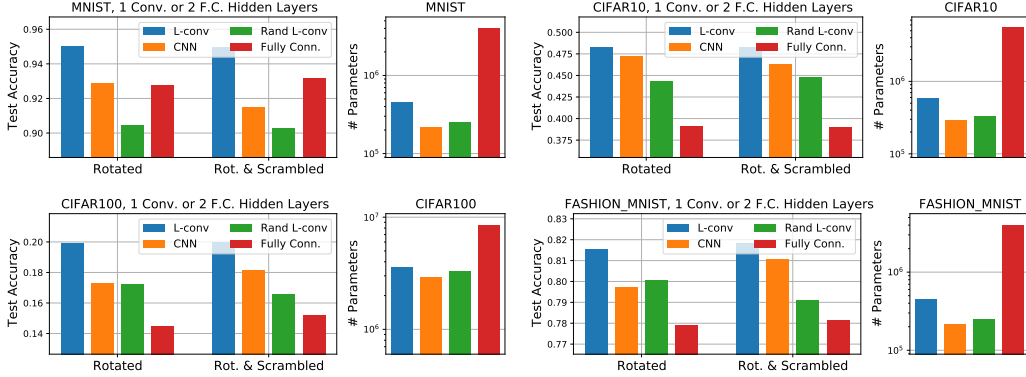


Figure 9: Results on four datasets with two variant: “Rotated” and “Rotated and scrambled”. In all cases L-conv performs best. On MNIST, FC and CNN come close, but using 5x more parameters.

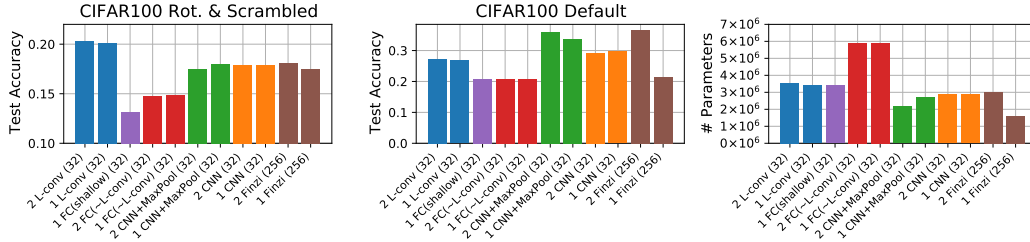


Figure 10: Comparison of one and two layer performance of L-conv (blue), CNN without pooling (orange), CNN with Maxpooling after each layer (green), fully connected (FC) with structure similar to L-conv (red), Lie-Conv (Finzi) Finzi et al. (2020) (brown), and shallow FC, which has a single hidden layer with width such that the total number of parameters matches L-conv (purple). The labels indicate number of layers, layer architecture and number of filters (e.g. “2 L-conv (32)” means two layers of L-conv with 32 filters followed by one classification layer). Left and middle plots show test accuracies on CIFAR100 with rotated and scrambled images, and on the original CIFAR100 dataset, respectively. The plot on the right shows the number of parameters in each model, which is the same for the two datasets.

and FashionMNIST, and on 50,000 CIFAR10 and CIFAR100 images. Scrambling destroys the correlations existing between values of neighboring pixels, removing the locality of features in images. As a result, CNN need to encode more patterns, as each image patch has a different correlation pattern.

**Test Model Architectures** We conduct controlled experiments, with one (Fig. 9) or two (Fig. 10) hidden layers being either L-conv or a baseline, followed by a classification layer. For CNN, L-conv and L-conv with random  $L_i$ , we used  $n_f = m_l = 32$  for number of output filters (i.e. output dimension of  $W^i$ ). For CNN we used  $3 \times 3$  kernels and equivalently used  $n_L = 9$  for the number of  $L_i$  in L-conv and random L-conv. We also used “LieConv” Finzi et al. (2020) as a baseline (Fig. 10, brown). We used the default  $k = 256$  in LieConv, which yields comparable number of parameters to our other models. For the symmetry group in LieConv we used  $SE(3)$ . We also used the default ResNet architecture provided by Finzi et al. (2020) for both the one and two layer experiments. We turned off batch normalization, consistent with other experiments. We encode  $L_i$  as sparse matrices  $L_i = U_i V_i$  with hidden dimension  $d_h = 16$  in Fig. 9 and  $d_h = 8$  in Fig. 10, showing that very sparse  $L_i$  can perform well. The weights  $W^i$  are each  $m_l \times m_{l+1}$  dimensional. The output of the L-conv layer is  $d \times m_{l+1}$ . As mentioned above, we use two FC baselines. The FC in Fig. 9 and FC( $\sim$ L-conv) in Fig. 10 mimic L-conv, but lacks weight-sharing. The FC weights are  $W = ZV$  with  $V$  being  $(n_L d_h) \times d$  and  $Z$  being  $(m_{l+1} \times d) \times d_h$ . For “FC (shallow)” in Fig. 10, we have one wide hidden layer with  $u = n_{L-conv} / (m d c)$ , where  $n_{L-conv}$  is the total number of parameters in the L-conv model,  $m$  and  $c$  the input and output channels, and  $d$  is the input dimension. We experimented with encoding  $L_i$  as multi-layer perceptrons, but found that a single hidden layer with linear activation works best. We also conduct tests with two layers of L-conv, CNN and FC (Fig. 10), with each

L-conv, CNN and FC layer as described above, except that we reduced the hidden dimension in  $L_i$  to  $d_h = 8$ .

**Baselines** We compare L-conv against four baselines: CNN, random  $L_i$ , fully connected (FC) and LieConv. Using CNN or  $SE(3)$  LieConv on scrambled images amounts to using poor inductive bias in designing the architecture. Similarly, random, untrained  $L_i$  is like using bad inductive biases. Testing on random  $L_i$  serves to verify that L-conv’s performance is not due to the structure of the architecture, and that the  $L_i$  in L-conv really learn patterns in the data. Finally, to verify that the higher parameter count in L-conv is not responsible for the high performance, we construct two kinds of FC models. The first type (“Fully Conn.” in Fig. 9 and “FC ( $\sim$  L-conv)” in Fig. 10) is a multilayer FC network with the same input ( $d \times m_0$ ), hidden ( $k \times n_L$  for low-rank  $L_i$ ) and output ( $d \times m_1$ ) dimensions as L-conv, but lacking the weight-sharing, leading to much larger number parameters than L-conv. The second type (“FC (shallow)” in Fig. 10) consists of a single hidden layer with a width such that the total number of model parameters match L-conv.

**Results** Fig. 9 shows the results for single layer experiments. On all four datasets both in the rotated and the rotated and scrambled case L-conv performed considerably better than CNN and the baselines. Compared to CNN, L-conv naturally requires extra parameters to encode  $L_i$ , but low-rank encoding with rank  $d_h \ll d$  only requires  $O(d_h d)$  parameters, which can be negligible compared to FC layers. We observe that FC layers consistently perform worse than L-conv, despite having much more parameters than L-conv. We also find that not training the  $L_i$  (“Rand L-conv”) leads to significant performance drop. We ran tests on the unmodified images as well (Supp. Fig 12), where CNN performed best, but L-conv trails closely behind CNN.

Additional experiments testing the effect of number of layers, number of parameters and pooling are shown in Fig. 10. On CIFAR100, we find that both FC configurations, FC( $\sim$ L-conv) and FC(shallow) consistently perform worse than L-conv, evidence that L-conv’s performance is *not* due to its extra parameters. L-conv outperforms all other tested models on rotated and scrambled CIFAR100, including LieConv. Without pooling, we observe that both L-conv and CNN do not benefit from adding a second layer. On the default CIFAR100 dataset, one and two layer CNN with max-pooling perform significantly better than L-Conv. Two Layer  $SE(3)$  LieConv (labelled “2 Finzi (256)”) performs best on default CIFAR100, but not on the scrambled and rotated version. This is expected, as the symmetries of the latter are masked by the scrambling. This is where the benefit of our model becomes evident, namely cases where the data may have hidden or unfamiliar symmetries. We also verified that the higher performance of L-conv compared to CNN is not due to higher number number of parameters (Appendix D.2)

## D.1 Details of experiments

**Hardware and Implementation** We implemented L-conv in Keras and Tensorflow 2.2 and ran our tests on a system with a 6 core Intel Core i7 CPU, 32GB RAM, and NVIDIA Quadro P6000 (24GB RAM) GPU. The L-conv layer did not require significantly more resources than CNN and ran only slightly slower.

### D.1.1 Comparison with related models

**Comparison with Meta-learning Symmetries by Reparameterization (MSR)** Recently Zhou et al. (2020) also introduced an architecture which can learn equivariances from data. We would like to highlight the differences between their approach and ours, specifically Proposition 1 in Zhou et al. (2020). Assuming a discrete group  $G = \{g_1, \dots, g_n\}$ , they decompose the weights  $W \in \mathbb{R}^{s \times s}$  of a fully-connected layer, acting on  $x \in \mathbb{R}^s$  as  $\text{vec}(W) = U^G v$  where  $U^G \in \mathbb{R}^{s \times s}$  are the “symmetry matrices” and  $v \in \mathbb{R}^s$  are the “filter weights”. Then they use meta-learning to learn  $U^G$  and during the main training keep  $U^G$  fixed and only learn  $v$ . We may compare MSR to our approach by setting  $d = s$ . First, note that although the dimensionality of  $U \in \mathbb{R}^{nd \times d}$  seems similar to our  $L \in \mathbb{R}^{n \times d \times d}$ , the  $L_i$  are  $n$  matrices of shape  $d \times d$ , whereas  $U$  has shape  $(nd) \times d$  with many more parameters than  $L$ . Also, the weights of L-conv  $W \in \mathbb{R}^{n \times m_l \times m_{l-1}}$ , with  $m_l$  being the number of channels, are generally much fewer than MSR filters  $v \in \mathbb{R}^d$ . Finally, the way in which  $Uv$  acts on data is different from L-conv, as the dimensions reveal. The prohibitively high dimensionality of  $U$  requires MSR to adopt a sparse-coding scheme, mainly Kronecker decomposition. Though not necessary, we too choose to use a sparse format for  $L_i$ , finding that very low-rank  $L_i$  often perform best. A Kronecker decomposition may bias the structure of  $U^G$  as it introduces a block structure into it.

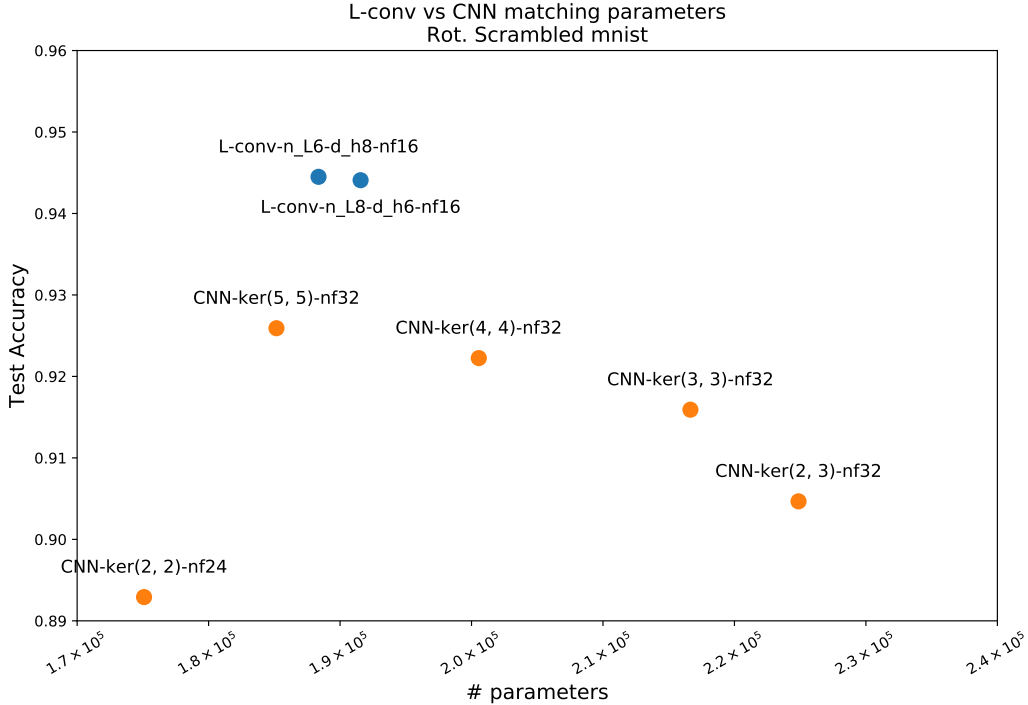


Figure 11: Matching number of parameters in CNN and L-conv, we observe that L-conv still performs better on Rotated and Scrambled MNIST.

**Contrast with Augerino** In a concurrent work, (Benton et al., 2020) propose Augerino, a method to learn invariances with neural networks. Augerino uses data augmentation to transform the input data, which means it is restricting the group to be a subgroup of the augmentation transformations. The data augmentation is written as  $g_\epsilon = \exp(\sum_i \epsilon_i \theta_i L_i)$  (equation (9) in Benton et al. (2020)), with randomly sampled  $\epsilon_i \in [-1, 1]$ .  $\theta_i$  are trainable weights which determine which  $L_i$  helped with the learning task. However, in Augerino,  $L_i$  are fixed *a priori* to be the six generators of affine transformations in 2D (translations, rotations, scaling and shearing). In contrast, our approach is more general. We learn the generators  $L_i$  directly without restricting them to be a known set of generators. Additionally, we do not use the exponential map, hence, implementing L-conv is very straightforward. Lastly, Augerino uses sampling to effectively cover the space of group transformations. Since the sum over Lie algebra generators is tractable, we do not need to use sampling.

## D.2 Additional Experiments

**Matching number of parameters in CNN** To verify that the difference in the number of parameters between CNN and L-conv was not responsible for the improved performance, we ran experiment where we allowed the kernel-size of L-conv and CNN to differ and tried to match the number of parameters between the two. Fig. 11 shows that on rotated and scrambled MNIST L-conv still performs better than CNN even after the latter has been allowed to have the same or more number of parameters than L-conv.

In Figure 13 we compare the performance of a single layer of L-conv on a classification task on scrambled rotated MNIST, where pixels have been permuted randomly and images have been rotated between  $-90$  to  $+90$  degrees. The models consisted of a final classification layer preceded by either one L-conv (blue), or one CNN (orange), or multiple fully-connected (FC, green) layers with similar number of neurons as the L-conv, but without weight sharing. We see that most L-conv configurations had the highest performance without a too many trainable parameters. Note that, parameters in FC layers are much higher than comparable L-conv, but yield worse results. The dots are labeled to show the configurations, with  $L[32]h[6](k[6])$  meaning  $k = 6$  as number of  $L_i$ , 32 output filters, and  $h = 6$  hidden dimensions for low-rank encoding of  $L_i$ . The y-axis shows the test accuracy and the

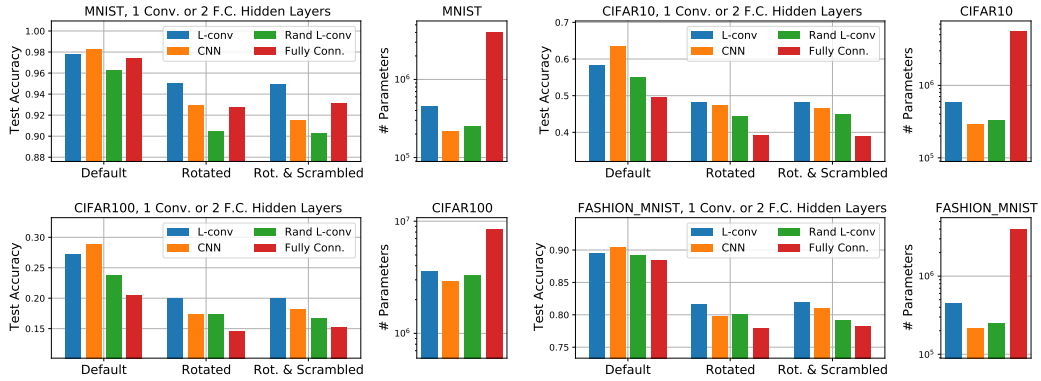


Figure 12: Test results on four datasets with three variant: “Default” (unmodified dataset), “Rotated” and “Rotated and scrambled”. On the Default dataset, CNN performs best, but L-conv is always the second best. For Rotated and Rot. & Scrambled, in all cases L-conv performed best. In MNIST, FC and CNN layers come close, but using 5x more parameters.

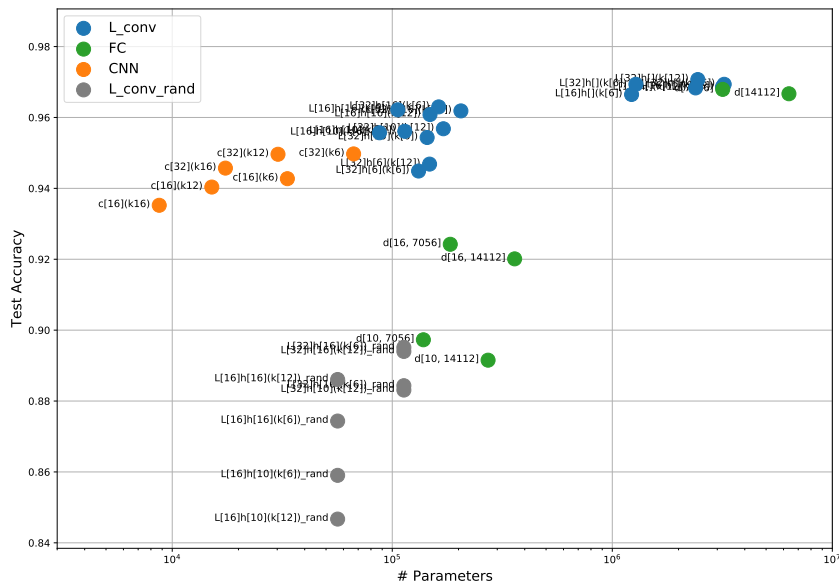


Figure 13: Training low-rank L-conv layer during training.

x-axis the number of trainable parameters. The grey lines show the performance of L-conv with fixed random  $L_i$ , but trainable shared wights, showing that indeed the learned  $L_i$  improve the performance quite significantly.